The Journal of Physiology

Evidence that interglomerular inhibition generates non-monotonic concentration-response relationships in mitral/tufted glomeruli in the mouse olfactory bulb

Lee Min Leong[1], David Wharton[2], Narayan Subramanian[1], Bhargav Karamched[2,3,4], Richard Bertram[2,3,4] and Douglas A. Storace[1,3,4]

[1]*Department of Biological Science, Florida State University, Tallahassee, Florida, USA*
[2]*Department of Mathematics, Florida State University, Tallahassee, Florida, USA*
[3]*Program in Neuroscience, Florida State University, Tallahassee, Florida, USA*
[4]*Institute of Molecular Biophysics, Florida State University, Tallahassee, Florida, USA*

Handling Editor: Nathan Schoppa

The peer review history is available in the Supporting Information section of this article (https://doi.org/10.1113/JP290366#support-information-section).

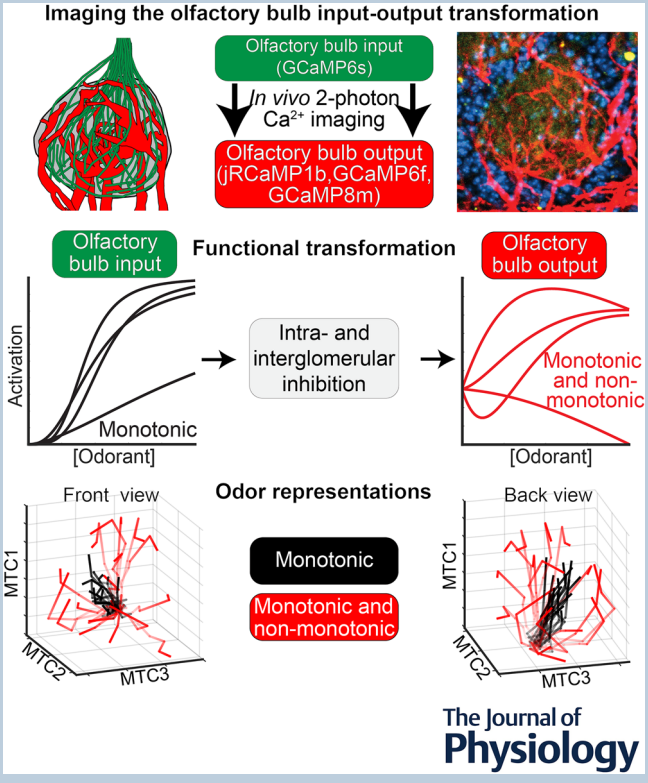

Abstract figure legend The olfactory bulb input–output transformation was imaged using dual-colour two-photon imaging. (*Top*) Cartoon and histological examples of labelling the olfactory bulb input and output using spectrally distinct optical sensors. (*Middle*) Modelling and experimental work reveal that input neurons that respond with primarily

L. M. Leong and D. Wharton have contributed equally to this work.

This article was first published as a preprint. Leong LM, Wharton D, Subramanian N, Karamched B, Bertram R, Storace DA. 2025. Evidence that interglomerular inhibition generates non-monotonic concentration-response relationships in mitral/tufted glomeruli in the mouse olfactory bulb. bioRxiv. https://doi.org/10.1101/2025.02.28.640652

 DOI: 10.1113/JP290366

monotonic concentration-response relationships are transformed into a mix of monotonic and non-monotonic responses. (*Bottom*) Olfactory bulb output state space for a population of three glomeruli with exclusively monotonic responses (black) and with both monotonic and non-monotonic responses (red). Each trajectory represents a cloud of points that reflects variations in the fluctuations of molecular components present in natural odour stimuli. Monotonic responses alone cluster together, whereas multiple response types broaden coverage of mitral and tufted cell (MTC) state space. Greater coverage of state space makes it easier to discriminate one odour from another, even though the dimension of olfactory bulb state space is greater than 3.

Abstract Animals can recognize an odour as the same odour across a range of concentrations and discriminate between odours in complex environments. Processing within the mouse olfactory bulb (OB) may be involved, yet the underlying mechanisms remain unclear. Each olfactory receptor neuron (ORN) type maps to the OB in olfactory receptor-specific channels called glomeruli, where they connect with the dendrites of mitral and tufted cells (MTCs), which project their axons to the rest of the brain. Modelling this transformation yielded predictions about how two kinds of inhibition, local intraglomerular and lateral interglomerular processing, shape MTC output as a function of concentration changes. We confirmed these predictions using *in vivo* single and dual-colour two-photon Ca^{2+} imaging from the ORNs and MTCs innervating the same glomeruli in the awake mouse OB in response to odours presented across a wide concentration range. We identified a transformation where concentration increases transformed ORN inputs with exclusively monotonically increasing responses into MTC outputs that non-monotonically increased then decreased, or vice versa. This transformation was odour-specific, consistent with rising levels of inhibition that scale with excitatory input and predicted by certain ORN characteristics. Therefore non-monotonic concentration-response relationships in MTCs are common and expected given how each glomerulus is shaped by feed-forward excitation, local and lateral inhibition. We propose that this transformation facilitates odour discrimination and the ability to achieve concentration-invariant odour perception by broadening MTC odour state space.

(Received 19 October 2025; accepted after revision 4 June 2026; first published online 25 June 2026)
Corresponding author D. A. Storace: Department of Biological Science, Florida State University, Tallahassee, FL 32306, USA. Email: dstorace@fsu.edu

Key points

- The role of the olfactory bulb in transforming sensory information remains poorly understood. In the bulb different olfactory receptor neuron (ORN) types map to olfactory receptor-specific channels called glomeruli, where they interact with the dendrites of mitral and tufted cells (MTCs), which project to the olfactory cortex.
- We developed a mathematical model detailing how different ORN inputs are transformed by intra-glomerular and lateral interglomerular inhibition as a function of odour concentration.
- Single- and dual-colour *in vivo* two-photon Ca^{2+} imaging of glomerular inputs and outputs across a wide concentration range confirmed some of the predictions.
- Increasing odour concentration transformed ORN inputs with monotonically increasing responses into non-monotonic MTC outputs, which responded with increases then decreases, or vice versa. This transformation is heterogeneous, odour-specific and predicted by certain ORN characteristics.
- This network transformation broadens the MTC odour state space, providing a mechanistic basis for achieving concentration-invariant odour perception and fine odour discrimination.

Introduction

The ability of an animal to detect and recognize odours is initiated by the binding of an odour ligand to olfactory receptor neurons (ORNs), each of which expresses one kind of olfactory receptor (OR) protein (out of ∼1000) and has a distinct affinity for each odour (Araneda et al., 2000; Buck & Axel, 1991; Malnic et al., 1999; Reisert

& Matthews, 1999; Xu et al., 2020; Zak et al., 2020). Odours evoke varying degrees of activity across the receptor population that must be related to perception. The relationship between ORs and their ligands follows classical ligand-receptor pharmacology, such that the activation of each OR type increases monotonically and saturates across a relatively narrow range of ligand concentration (Bozza et al., 2002; Firestein et al., 1993; Ma et al., 1999; Reisert & Matthews, 1999). This has an important implication for olfactory processing and perception: the population ORN response to an odour will change when it is experienced at different concentrations or in presence of other odours. Low concentrations of an odour will activate receptors with high sensitivity to that odour, whereas higher concentrations of the same odour will saturate high affinity ORs and recruit OR types with lower sensitivity to that odour (Hu et al., 2020; Storace & Cohen, 2017; Storace et al., 2019; Wachowiak & Cohen, 2001). Without further processing an organism could not recognize or discriminate between odours in a concentration-invariant manner.

Each ORN type provides input to the olfactory bulb (OB) in OR-specific channels called glomeruli (Buck & Axel, 1991; Malnic et al., 1999). Mitral and tufted cells (MTCs) extend their apical dendrite into a single glomerulus and project their axons to the rest of the brain (Chen et al., 2022; Igarashi et al., 2012; Nagayama et al., 2010). Therefore each glomerulus contains the input–output transformation for a given OR type, which can be influenced by a complex synaptic network that includes inhibitory interneurons and feedback from other brain regions (Cleland, 2010; Cleland & Sethupathy, 2006; Nagayama et al., 2014; Parrish-Aungst et al., 2007).

Although OB processing is involved in generating concentration-invariant odour representations, the underlying mechanisms remain unclear (Storace & Cohen, 2017; Storace et al., 2019). To address this knowledge gap we used a mathematical model of the OB input–output transformation to begin to yield predictions about how different ORN input types interact with local intraglomerular and lateral interglomerular inhibition to transform MTC outputs. We confirmed some of the model predictions using *in vivo* single and dual-colour two-photon Ca^{2+} imaging from the ORN axon terminals and the MTC apical dendrites innervating the same glomeruli (hereafter referred to as ORN and MTC glomeruli).

Experimentally increasing odour concentration increased the number of odour-responsive glomeruli, which were either excited or suppressed by the odour stimulus. Notably ORN inputs with monotonic concentration-response relationships were transformed into non-monotonic MTC outputs that responded to increasing concentration with response amplitudes that either increased then decreased or vice versa. Because non-monotonic concentration-response relationships are unexpected in a system driven by ORN input, they indicate a transformation occurring within the OB that has implications for coding principles and the mechanisms underlying this process.

Indeed these changes were accompanied by rising levels of suppression across the glomerular population, which is consistent with graded activation of inhibitory networks. Additionally our modelling results indicate that the two kinds of responses are consistent with OB processing via two kinds of inhibition: local intraglomerular and lateral interglomerular processing, in which the MTC output reflects a combination of its afferent input, as well as the collective activity across a population (Carandini & Heeger, 2011; Cleland et al., 2007; Olsen et al., 2010). Consistent with the model predictions the specific MTC response type was odour- and glomerulus-specific and, importantly, predicted by specific ORN characteristics.

Therefore non-monotonic MTC concentration-response relationships are an expected consequence of how ORNs with limited dynamic range interact with rising levels of local and lateral inhibition. As the concentration of a particular odour is increased, the responses of ORNs with high sensitivity to that odour will compress as they reach the upper limits of their dynamic range, whereas less-sensitive ORNs will become activated. The consequence is that MTCs innervated by high-sensitivity ORNs will be weakened by rising levels of lateral inhibition, and those innervated by low-sensitivity ORNs will be suppressed. Our results provide direct evidence of a functional transformation occurring across the OB network. We propose that the presence of non-monotonic concentration-response relationships provides a mechanism to facilitate odour discrimination and concentration-invariant odour perception.

Lee Min Leong is a postdoctoral researcher at Florida State University. Transitioning from engineering genetically encoded voltage indicators to their *in vivo* application her current project utilizes imaging techniques to investigate the transformation processes within the olfactory bulb to better understand how the brain converts sensory signals into neural representations of odour.

Methods

A subset of these data were included in a previous publication that analysed the adapting properties of MTC odour responses (Subramanian et al., 2025).

Ethical approval

All experiments were carried out according to the procedures and guidelines approved by the Florida State University Animal Care and Use Committee under ethics approval reference #202100074.

Mathematical modelling

The model is based on ideas described in Cleland and Sethupathy (2006) and incorporates two forms of inhibition: local and lateral. The output of the ORNs is dependent upon the odorant concentration, [odorant], and is described mathematically by the sigmoidal Hill function:

$$\mathrm{ORN} = \frac{\upsilon\,[\mathrm{odorant}]^n}{\kappa^n + [\mathrm{odorant}]^n} \tag{1}$$

All variables and parameters are dimensionless, and [odorant] ranges from 0 to 1. The parameter υ sets the maximum value of ORN and is assumed to be the same for all ORNs. The other two parameters are the half-activation constant, κ, and the Hill coefficient, n, which sets the steepness of the ORN's response (higher values of n yield steeper response functions). To generate a large ($N = 949$) heterogeneous population of ORNs N combinations of parameter values were sampled from a uniform distribution on the intervals of (0,2) for κ and (1,4) for n. The ORN signal is then subject to presynaptic inhibition from other glomeruli before entering the target glomerulus, producing a 'normalized ORN' value $\overline{\mathrm{ORN}}$:

$$\overline{\mathrm{ORN}} = \frac{\mathrm{ORN}}{1+\mu} \tag{2}$$

where $\mu = \sum_{i=1}^{M} \mathrm{ORN}_i/M$ is the average ORN activity over a population ORNs. We consider two cases. In the first case each ORN is normalized by a randomly selected population of $M = 50$ ORNs. In the second case each ORN is normalized by all other $M = 948$ ORNs. This normalized output of the ORN is then the input to periglomerular and MTCs, reflected in the variables PG and MTI, respectively. The circuitry involved in this lateral inhibition is not specified in the model and could reflect the action of short axon cells onto external tufted cells, which then serve as input to MTCs and PG cells, as previously described (Banerjee et al., 2015; McGann, 2013).

Table 1. Parameter values used in model simulations

Symbol	Value(s)	Description
[odorant]	[0,1]	Concentration of input stimuli
υ	2	Maximum ORN value
n	Random(1,4)	ORN Hill coefficient
κ	Random(0,2)	ORN half-activation value
β	0.6	Maximum PG value
κ_p	0.5	PG half-activation value
κ_m	1	MTI half-activation value

The PG and MTI variables are described with increasing Hill functions:

$$\mathrm{PG} = \frac{\beta\,\overline{\mathrm{ORN}}^{4.5}}{\kappa_p^{4.5} + \overline{\mathrm{ORN}}^{4.5}} \tag{3}$$

$$\mathrm{MTI} = \frac{\overline{\mathrm{ORN}}^{3}}{\kappa_m^{3} + \overline{\mathrm{ORN}}^{3}} \tag{4}$$

where β, κ_p and κ_m are parameters that are assumed to be the same for each PG and MTI. They are set so that PG begins to activate at lower values of $\overline{\mathrm{ORN}}$ than MTI and saturates at a lower value (saturation value of β) than MTI (saturation value of 1). The higher affinity of PG cells is a key element of the half-hat coding hypothesized by Cleland (Cleland, 2010; Cleland & Sethupathy, 2006). The output of each glomerulus, MTC output, is then the difference between MTI and the inhibition from PG cells:

$$\text{MTC output} = \mathrm{MTI} - \mathrm{PG} \tag{5}$$

Parameter values are given in Table 1.

Transgenic mice

GCaMP6f was targeted to MTC glomeruli by mating the Ai148 GCaMP6f transgenic reporter line (Jax stock #030328) to the Tbx21-cre transgenic line (Jax stock #024507) (Daigle et al., 2018; Mitsui et al., 2011; Subramanian et al., 2025). GCaMP6s was targeted to ORN glomeruli by mating the tetO-GCaMP6s transgenic reporter line (Jax stock #024742) to the OMP-tTA transgenic line (Jax stock #017754) (Huang et al., 2022; Subramanian et al., 2025). This OMP-tTA-tetO-GCaMP6s line was mated with the Tbx21-cre transgenic line (Jax stock #024507) to create a triple-transgenic line (OMP-tTA-tetO-GCaMP6s Tbx21-cre), expressing GCaMP6s in the ORN glomeruli and allowing for Cre-dependent expression in the MTC glomeruli. GCaMP8m was targeted to MTC glomeruli by mating the TIGRE2-jGCaMP8m-IRES-tTA2-WPRE transgenic

reporter line (Jax stock # 037718) to the Tbx21-cre transgenic line (Jax stock #024507) (Daigle et al., 2018; Mitsui et al., 2011; Subramanian et al., 2025). Genotyping was performed by Transnetyx (Cordova, TN, USA), and adult male and female offspring expressing eGFP and Cre recombinase in MTC glomeruli or eGFP, tTA and Cre recombinase in ORN glomeruli were used for experiments. We further confirmed that the fluorescent proteins were expressed in the excepted cell population in histological samples (described under Histology).

Surgical procedures

All procedures were approved by the Florida State University Animal Care and Use Committee. All mice included in this study were maintained in the FSU animal vivarium on a 12h/12h light/dark rhythm with *ad libitum* access to food and water. Adult male and female (> 21 days) transgenic mice were anaesthetized using ketamine/xylazine (90/10 mg/kg, IP, Zoetis, Kalamazoo, MI, USA), placed on a heating pad and had ophthalmic ointment applied to their eyes. Mice were given a pre-operative dose of carprofen (20 mg/kg, SC, Zoetis), atropine (0.2 mg/kg, IP, Covetrus, Dublin, OH, USA), dexamethasone (4 mg/kg, IP, Bimeda, La Sueur, MN, USA) and bupivacaine (1.5 mg/kg, SC, Hospira, Lake Forest, IL, USA). Fur was removed from the top of the skull using a depilatory agent and rinsed, after which the skin was scrubbed with 70% isopropyl alcohol and iodine (Covidien, Mansfield, MA). An incision was made to remove the skin over the skull, and blunt dissection was used to remove the underlying membrane. Dental cement (Metabond) was used to attach a custom headpost to the skull, which was held using a custom headpost holder. After the cement finished drying the bone above the OB was either thinned using a dental drill (Osada, XL-230, Los Angeles, CA, USA) and covered with cyanoacrylate to improve optical clarity or was removed and replaced with cover glass.

For the dual-colour input–output experiments stereotaxic injections were carried out immediately after the craniotomy. A total of 500 nl of AAV1.Syn.Flex.NES-jRCaMP1b.WPRE.SV40 (Addgene, 100850-AAV1, Watertown, MA, USA) was injected into the right OB of OMP-tTA-tetO-GCaMP6s; Tbx21-cre triple-transgenic mice before the cranial window was sealed with a #1 cover glass. Upon completion of the surgery the mouse was allowed to recover on a heating pad until they were fully ambulatory. Animals were given a postoperative dose of carprofen (20 mg/kg, SC) at the end of the day of surgery and for at least 3 days postoperatively. The AAV was allowed to express for at least 2 weeks before imaging experiments began.

Histology

We validated the targeting of the optical sensors used in this study based on endogenous fluorescence expression of GCaMP6f (MTCs), GCaMP6s (ORNs), GCaMP8m (MTCs) and jRCaMP1b (MTCs). Histological samples were observed using appropriate filter sets using a Zeiss Axioskop epifluorescence microscope and were imaged on a Nikon CSU-W1 spinning disk confocal microscope using 10 × 0.45 N.A., 40 × 0.95 N.A. or 40 × 1.15 N.A. objective lenses. Euthanasia was carried out via procedures approved by the FSU ACUC. Mice were killed via an IP injection of euthasol and either underwent cardiac perfusion with phosphate-buffered saline and 4% paraformaldehyde or had their brains directly extracted and postfixed in 4% paraformaldehyde before being cut on a vibratome in 40 μm sections (Leica VT1000S, Deer Park, IL, USA). OB sections were mounted on slides and were cover-slipped using Fluoromount-G containing DAPI (SouthernBiotech, Birmingham, AL, USA).

Two-photon imaging

Imaging was performed using a Sutter MOM two-photon microscope equipped with an 8 kHz (30.9 Hz) resonant scanner (Cambridge Technology, Bedford, MA, USA) and an emission pathway equipped with a GaAsP PMT (#H10770PA-40-04, Hamamatsu, Japan). Laser excitation was provided using either an Alcor 920–2W laser (920 nm for GCaMP imaging) with power modulated by an internal acousto-optic modulator or a Spectra-Physics DS+ between 940 and 980 nm for GCaMP imaging or 1100 nm for jRCaMP1b imaging, with power modulated by a Pockels cell (Model #350-105-02, Conoptics, Danbury, CT, USA). Imaging was performed using a Nikon 16 × 0.8 N.A. or a 10 × 0.5 N.A. objective lens (Yu et al., 2024). Laser power was confirmed to be less than 150 mW at the output of the objective lens, as measured using a power meter (Newport 843-R) for scanning areas ranging between 711 and 1138 μm^2.

Odorant delivery

Methyl valerate (99% pure, CAS #624-24-8, Sigma-Aldrich, #148997), isoamyl acetate (99% pure, CAS #123-92-2, Thermo Scientific #150662500), benzaldehyde (> 99.5% purity, CAS #100-52-7, Sigma Aldrich #418099), acetophenone (99% pure, CAS #100-52-7, Fisher Scientific #AAA12727AP) and 2-phenylethanol (> 99% CAS #60-12-8, Sigma-Aldrich #77861) were used at concentrations between 0.05% and 5.5% of saturated vapour. The olfactometer design involved air being pushed through vials of pure odour using a syringe pump (NE-1000, PumpSystems, Farmingdale, NY, USA) running at different flow rates (0.25–28

mL/min) (Subramanian et al., 2025). This odour stream underwent an initial air dilution with a lower flow rate of clean air (30 mL/min). The resulting odorized air stream was connected to a dual three-way solenoid valve (360T041, NResearch, West Caldwell, NJ, USA), which was connected to an exhaust, a clean air stream and a Teflon delivery manifold, which served as the final delivery apparatus placed in front of the mouse's nose. The delivery manifold had a higher flow rate of clean air constantly flowing through it (450 mL/min), which provided a second air dilution. At rest the solenoid sent the odorized air stream to the exhaust and the clean air stream to the animal; odour delivery occurred by triggering the solenoid, which caused the odour to be injected into the delivery manifold.

For the dual-colour input–output experiments the odorants methyl valerate, isoamyl acetate, acetophenone and methyl salicylate (99% pure, CAS#119-36-8, Sigma-Aldrich #M2047) were diluted in mineral oil to 0.002%, 0.008%, 0.046%, 0.278%, 1.667% and 10%. The olfactometer set-up uses an air pump that is constantly delivering clean air to two mass flow controllers (MC-100SCCM and MC-1SLPM, Alicat, Tucson, AZ, USA).

The odour mass flow controller (MC-100SCCM) controls the air flow that passes through the odour vials (50 mL/min for this study), the dilution mass flow controller (MC-1SLPM) provides a higher flow rate of air (450 mL/min for this study) that dilutes the odorized air (i.e. the odours were delivered at 10% saturated vapour). The mass flow controllers are each connected to a four-valve manifold (360T081, NResearch), where the odour vials are connected in between. At any given time only one of the four pairs of manifold valves open to allow for the odour air stream to blend with the dilution air stream to deliver a particular concentration of the mineral oil-diluted odours. The resulting odorized air stream was connected to a dual three-way solenoid valve (360T041, NResearch), which was connected to an exhaust, a clean air stream and a Teflon delivery manifold, which served as the final delivery apparatus placed in front of the mouse's nose. The delivery manifold has a separate air pump that delivers clean air at a flow rate that is matched to the flow rate output of the mass flow controllers. The three-way solenoid valve sends the odorized air stream to the exhaust and the clean air stream to the mouse prior to odour trigger. Triggering the three-way solenoid causes the odour to be injected into the delivery manifold. The odour delivery time course for both olfactometer setups were confirmed using a photoionization detector (200C, Aurora Scientific, Aurora, ON) (Storace & Cohen, 2017, 2021; Subramanian et al., 2025).

Imaging procedures

Before data collection mice were positioned underneath the microscope, and the headpost holder angle was adjusted to optimize the imaging field of view. During data collection awake head-fixed mice were placed underneath the microscope objective with the olfactometer and either a thermocouple (Omega 5TC-TT-K-36-36, Michigan City, IN, USA) near its nose, or a pressure sensor embedded in the olfactometer, to measure respiration. The signals from the respiration sensor were amplified and low-pass filtered using a differential amplifier (Model 3000, AM-Systems, Sequim, WA, USA), which was recorded by the imaging system. For GCaMP6f imaging experiments (Figs 2–6) odours were delivered at concentrations between 0.05% and 5.5% of saturated vapour in trials separated by a minimum of 3 min. For glomerular imaging using jGCaMP8m (MTCs), jRCaMP1b (MTCs) and GCaMP6s (ORNs) odours were delivered in six concentration steps between 0.002% and 10% of pure odour diluted in mineral oil at 10% of saturated vapour and air trials in which the odour stream was passed through a previously unused vial. For each animal we prioritized measuring multiple repetitions for each concentration for a particular odour before a second odour was attempted.

Data analysis

Frame subtraction analysis. The mean fluorescence and frame subtraction images are from the average of at least two single trials (Figs 2*A* and 7*C*). The mean fluorescence images are generated from the average of all the frames during the imaging trial or all the frames prior to odour stimulation. The frame subtraction images were generated by subtracting an average of the 19 frames during odour stimulation from the average of 9 frames prior to the stimulus. The resulting image underwent two passes of a low-pass spatial filter, and the fluorescence (F) values were converted to $\Delta F/F$ by dividing the fluorescence value of each pixel by the mean of at least 60 consecutive frames in the image stack in Turbo-SM software (SciMeasure, Decatur, GA, USA). The intensity scale range is fixed to the same minimum and maximum range for all concentrations for each odour (Fig. 2).

Processing and segmentation. After data acquisition the raw image files were spatially and temporally averaged from 512 × 512 pixels sampled at 30.9 Hz to 256 × 256 pixels sampled at 7.72 Hz.

The resulting data were exported to TIFF format for all subsequent analysis. Occasional recordings with motion artifact that made it impossible to interpret the measurements were discarded from subsequent

analysis. Glomerular regions of interest were manually segmented using Turbo-SM software (SciMeasure, Decatur, GA, USA) and were identified based on their morphological properties in the mean fluorescence and functional responses in a frame subtraction. The pixel areas containing the regions of interest were saved, and the fluorescence time course values from each region of interest were extracted for subsequent analysis. Fluorescence time course values were converted to $\Delta F/F$ by dividing each trace by the mean of the frames prior to odour stimulation. Odour response amplitudes and corresponding *z*-scores were calculated as the largest difference between a 1200 ms window during the odour presentation and the time prior to odour stimulation.

Other analyses. Population descriptive statistics were quantified in responsive glomeruli, which were defined as those in which an odour evoked a minimum 5 SD change from baseline at any concentration (Fig. 2*F*). Threshold and best response are defined as the lowest concentration evoking a response and the concentration evoking the largest response, respectively (Fig. 2*G* and *H*).

For all other analyses glomeruli were included that responded with a minimum of 3 SD above baseline at some concentration. The response category assigned to each MTC glomerulus was defined based on a combination of visual inspection of the mean concentration-response curve, the corresponding single trials and the *z*-score change in response to the odour stimulus. Excited and suppressed glomeruli were defined based on having clear odour-locked increases or decreases that could be clearly identified in the mean and single-trial fluorescence time course. Population measurements of the different response categories were generated by averaging the fluorescence time course from all the glomeruli in a field of view assigned to that category (Fig. 3*E* and *F*).

For the spatial maps of glomerular $\Delta F/F$ and categorical responses glomeruli that did not respond at any concentration are indicated using cross-hatching (Fig. 4*A* and *B*). For responsive glomeruli concentrations that evoked a change of less than 2 SD were assigned a value of zero to facilitate visual analysis (Fig. 4*A*, white polygons). For the network category analysis (Fig. 4*B* and *C*) the response category of each glomerulus was included for preparations that were tested to more than one odour. The network graph in Fig. 4*C* was generated by plotting the categories of each glomerulus for different odours using the graph function in MATLAB.

The relationship between excitation and suppression was quantified by averaging the response from all glomeruli that responded to the highest concentration with excitation and suppression, respectively (Fig. 5). The mean excited and suppressed responses for each preparation are plotted together, with the responses from individual preparations connected with a line (Fig. 5*E*). The correlation between these values was quantified for individual preparations and across the population using the corrcoef function in MATLAB (Fig. 5*D* and *E*). The variance explained was quantified by binning the mean excitation and suppression value measured for each concentration (Fig. 5*E*, black continuous line) and fitting them with a sigmoid (Fig. 5*E*, black dashed line) (Economo et al., 2016).

To avoid biasing the proportion of the dataset identified as non-monotonic we analysed the GCaMP6f dataset using two approaches. The first approach used the monotonicity index (MI), a metric that computes the degree of non-monotonicity in a concentration-response function (CRF; Fig. 6) (Escabí et al., 2007; Higgins et al., 2008). The MI of individual glomeruli was calculated by computing the d-prime value by measuring the CRF in $\Delta F/F$.

$$D' = \frac{\mathrm{CRF} + \mathrm{CRF}_{\max}}{\sqrt{\sigma^2_{\max} + \sigma^2}} \tag{6}$$

The $\mathrm{CRF}_{\max}$ is the response at the concentration with the largest $\Delta F/F$ change from the baseline, and CRF is the $\Delta F/F$ change at each concentration. $\sigma^2{}_{\max}$ is the response variance at the highest odour concentration, whereas σ^2 is the response variance at each odour concentration. MI was then computed as the minimum *D*' measured at concentrations beyond the one evoking the maximum $\Delta F/F$ response. Consequently a monotonically increasing glomerulus is assigned a value of 0, whereas glomeruli with non-monotonic concentration response functions are assigned negative values. Glomeruli with moderate non-monotonic shapes are closer to 0, whereas those with a larger decrease are assigned increasingly negative values. For the analysis in Fig. 6 MI values were quantified for all glomeruli in the GCaMP6f dataset except for exclusively suppressed glomeruli, because they are assigned large MI values. The second approach quantified the general slope of the MTC CRF (Shen et al., 2025). The linear slope of MTC glomeruli was quantified by first performing a linear interpolation between each consecutive pair of points in the concentration-response relationship. The polyfit function in MATLAB was then used to find the average slope of each line.

Half-maximum values were quantified by performing a linear interpolation of the concentration-response relationship for each glomerulus (linearinterp fittype in MATLAB) (Figs 6 and 7, vertical lines). The half-maximum value was defined as the concentration evoking the half-maximum response in the linear interpolation, except for the caveat in which glomeruli with a response to the lowest concentration that was greater than the half-maximum response were assigned a half-maximum value of 0.05% (e.g. Fig. 6*B*, roi9).

Hill equation fits of monotonically increasing glomeruli were performed in glomeruli exhibiting MI values greater than −0.5. Hill fits were calculated using the following equation where X is the response (in $\Delta F/F$) of the glomerulus at each concentration, and k is the half-saturating value estimated from a linear interpolation of the CRF.

$$\frac{X^n}{X^n + k^n} \tag{7}$$

Fits were analysed only if they met the following criteria: the Hill coefficient was between 0.75 and 6; the r^2 value was greater than 0.9, the root mean sum of squares was less than 0.1 and the sum of square error was less than 0.1 (Zak et al., 2020).

The trajectory plots were generated by plotting the odour response amplitudes of three glomeruli exhibiting exclusively increasing responses, or a combination of all response categories using the plot3 function in MATLAB (Fig. 10). Data are presented as mean ± SD. All error bars represent SD.

Results

To understand the transformation of sensory inputs in the OB we first developed a predictive model to establish how different kinds of inhibition transform ORN inputs (Figs 1 and A1). We used single-colour *in vivo* two-photon imaging to characterize the broad network responses and test key model predictions (Figs 2–6, A2 and A3). Finally we used a novel dual-colour two-photon imaging approach to directly link specific ORN inputs to their corresponding MTC outputs to confirm our mechanistic hypothesis (Figs 7–9).

Predictions from a model of the OB that combines intra- and interglomerular processing

We generated a model to better understand how intra- and interglomerular processing transforms the concentration-response properties of different ORN inputs (see Methods for model equations and parameter values). The output of each glomerulus (Fig. 1*Ad*) was a function of its ORN input (Fig. 1*Aa*), input from local interneurons that are activated by ORN input and provide inhibition onto the MTC output (Fig. 1*Ab*) and inhibitory interglomerular connectivity acting presynaptically to the MTCs (Fig. 1*Ac*). ORNs modelled using the Hill equation served as input to both MTCs and inhibitory intra-glomerular interneurons whose activation was described by a Hill function left-shifted relative to the MTC response function (Fig. 1*B*, PG). The difference between these two response functions was then taken as the output from the MTC (Fig. 1*B*, MTC output). The MTC output, which is relative to the basal level of activity, has a half-hat shape that shows a dip to negative values for low ORN activation and an increase for higher ORN activation, as previously described by Cleland (Fig. 1*B*, MTC output) (Cleland & Sethupathy, 2006).

Interglomerular processing was modelled by generating a population of 949 ORNs, with Hill coefficients sampled from a uniform distribution from 1 to 4, consistent with previously published work (Fig. 1*C*, coloured thin lines) (Firestein & Zufall, 1993; Platisa et al., 2022; Storace & Cohen, 2017; Wachowiak & Cohen, 2001; Zak et al., 2020). Odour sensitivities (their half-maximum values) were sampled from a uniform distribution on the interval between 0 and 2 (Fig. 1*C*). The model is dimensionless, as are the half-maximum values for the receptors. The ORN input to the MTCs and inhibitory PG cells was divided by the mean ORN activity over a population of 50 randomly selected ORNs to reflect lateral inhibition from a small subset of the glomeruli. This structure results in a normalization procedure in which the outputs of each MTC glomerulus are influenced by the input from a randomly selected subset of ORN glomeruli (Carandini & Heeger, 2011). One example of a normalizing function is shown as a dashed curve in Fig. 1*C*.

Four examples of ORN input and corresponding MTC output across a concentration range are illustrated in Fig. 1*D* (the colours are matched across the two subpanels). The model output in response to four input functions could be broadly described as having concentration-response relationships that monotonically increased (I), monotonically decreased (D), transitioned from suppressed to excited (DI) or increased to a point at which further increases in concentration evoked progressively smaller responses (ID) (Fig. 1*D*, right sub-panel).

The types of MTC responses are shown with colour coding in Fig. 1*E* (left) over a grid of values of the ORN Hill coefficient and half-activation constants. The ORNs with the highest sensitivities to an odour had a purely decreasing response to increasing odour concentrations (Fig. 1*D* and *E*, top red regions). In these cases the MTC output reached its maximum at low odour concentrations and could only decline due to lateral inhibition as other glomeruli became activated at higher concentrations. For ORNs with lower but still relatively high sensitivities the typical response was an initial increase followed by a decrease (Fig. 1*E*, ID, blue region). In these cases strongly activated ORNs near saturation were dominated by increasing lateral inhibition. For lower-sensitivity ORNs the response was purely increasing, particularly when the ORN response function was relatively linear (Fig. 1*E* and *I*, black region). At even lower sensitivities the typical response was a decrease followed by an increase (Fig. 1*E*, DI, green region). In this case inhibition dominated the MTC output prior to its strong activation

at higher odour concentrations, producing a DI response. Finally at the lowest sensitivities the response was purely decreasing, reflecting dominance of inhibition over all odour concentrations considered (Fig. 1*D* and *E*, red region).

In principle D responses can be generated by feed-forward suppression within a range of concentrations (e.g. Fig. 1*B*, dashed line between 0 and 0.6) or in the case of spontaneously active ORNs suppressed by inter-glomerular inhibition. However ID responses cannot

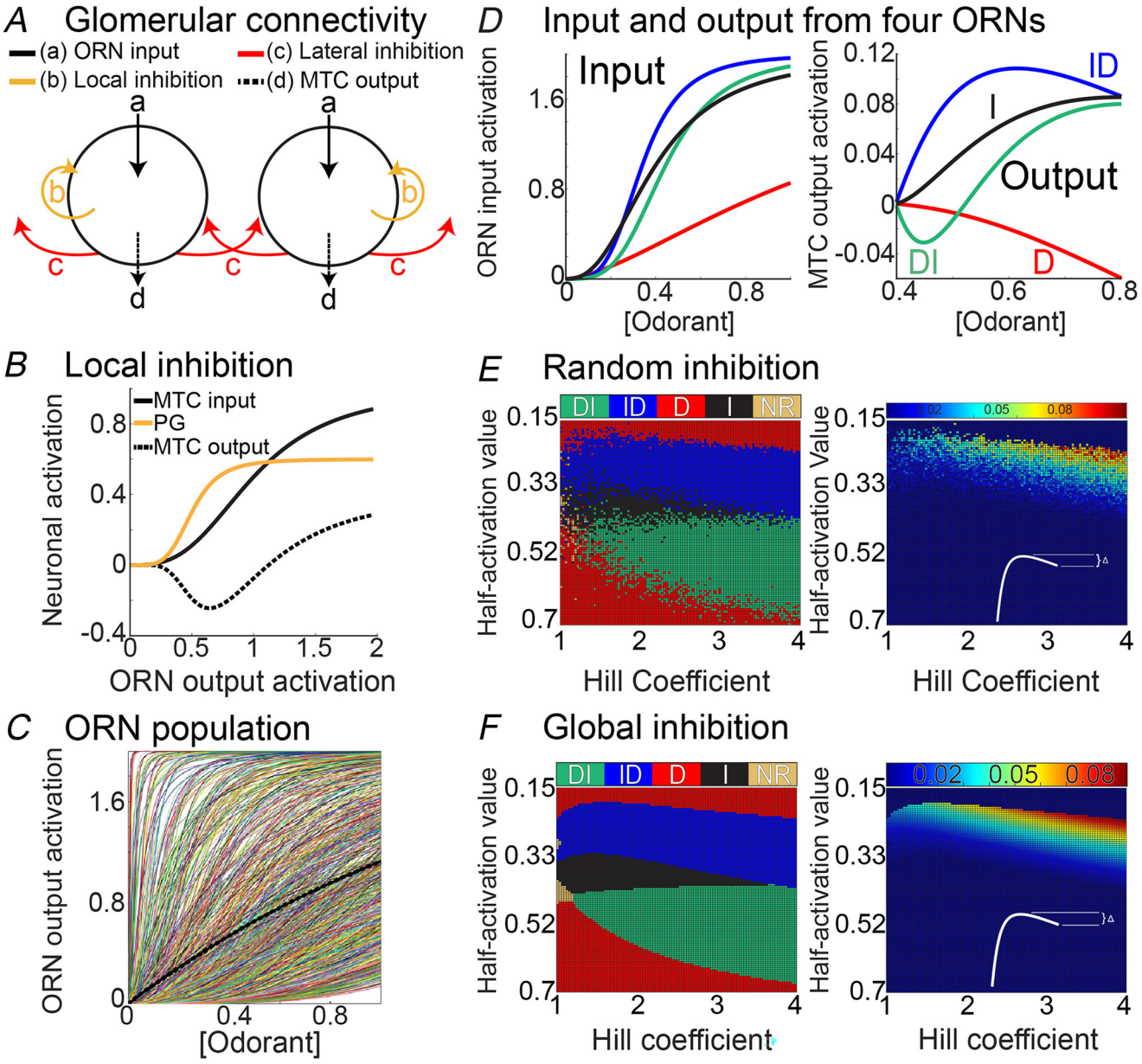

Figure 1. Modeling the olfactory bulb input-output transformation
A, glomerular connectivity in the model. *B*, local inhibition alone generates a half-hat response in mitral and tufted cells (MTCs). *C*, the population of 949 olfactory receptor neurons (ORNs) used in the model. One example of a normalizing curve is shown (dashed). *D*, the concentration-response relationships of four ORNs (left) and their corresponding MTC output (right) reflecting both local and lateral inhibition. Output responses were categorized based on the shape of the concentration-response relationship: I, increasing; ID, increasing then decreasing; DI, decreasing then increasing; D, decreasing. *E*, (left) MTC responses for different ORN Hill coefficients and half-activation values, in which normalization of input into each glomerulus is through a randomly selected sub-population of 50 glomeruli. (right) The decrease from the maximum to the terminal odorant concentration value for combinations of Hill coefficients and half-activation values that result in an ID response. *F*, similar to the previous panel but now normalization of input into each glomerulus is through all other glomeruli.

result from the local inhibition motif used in our model. Instead they depend upon lateral inhibition, which we hypothesize results from higher levels of interglomerular inhibition resulting from the activation of ORN glomeruli with lower sensitivities to the odour. We tested this hypothesis by excluding lateral inhibition from the model, which resulted in a loss of the ID response types (Fig. A1*A* and *B*).

A consequence of this framework is that the magnitude of non-monotonicity should be heterogeneous and originate from higher-affinity glomerular input that saturates at lower concentrations. A quantification of the decrease in MTC activation from the maximum over the grid of ORN parameters evoking ID responses revealed a gradient of non-monotonic drops (Fig. 1*E*, right). Most of the parameter values in the grid that produced a large drop in MTC activation following a peak had small ORN half-activation values, indicating high sensitivity for the odour.

The structure of the interglomerular inhibitory network is currently unknown (Banerjee et al., 2015; Economo et al., 2016; Fantana et al., 2008). The results shown in Fig. 1*E* were obtained assuming that each glomerulus is subject to lateral inhibition from a subpopulation of 50 randomly selected glomeruli. When the subpopulation was increased to include all glomeruli, so that there is all-to-all coupling among the glomeruli, the results are qualitatively similar (Fig. 1*F*). With this larger normalizing population the boundaries between the different response categories become sharper, but the basic structure of the response pattern is the same. In general we found that the main effect of reducing the size of the randomly selected normalizing set of glomeruli was to increase the fuzziness of the boundaries between the different response regions. We also considered the case in which input from 5 and 10 randomly chosen glomeruli provided the interglomerular inhibition, which resulted in different average ORN activation curves (Equation 2) (Fig. A1*C*). Importantly all four types of response patterns were produced when interglomerular processing was implemented with the random subsets of ORNs (Fig. A1*D*). It is clear, then, that the four different response types are generic, whereas the shapes and extent of the regions in the two-parameter grid that produce the different types of responses depend on the structure of the interglomerular inhibitory network.

In vivo measurements of concentration-response relationships in MTC glomeruli

We tested these predictions in a dataset in which odour responses were measured from MTC glomeruli across a ∼100-fold change in concentration using *in vivo* two-photon Ca^{2+} imaging in awake mice. Imaging was performed in transgenic mice in which GCaMP6f was selectively expressed in MTCs and their corresponding apical dendrites innervating the glomerular layer (Fig. 2*A*, mean fluorescence). We histologically confirmed targeting of GCaMP6f to MTCs in three preparations (not shown, but see Subramanian et al., 2025). Frame subtraction analyses from different preparations illustrate that odours evoked different patterns of excited and suppressed responses within the same field of view (Fig. 2*A*, white *vs*. black regions in frame subtractions). The specific activation pattern across the glomerular population was a complex function of odour concentration (Fig. 2*A*, compare over concentration range 0.05%–5.5%). Many glomeruli became increasingly excited (monotonically increasing, I) or suppressed (monotonically decreasing, D) at higher concentrations (Fig. 2*A*, I *vs*. D). Some glomeruli exhibited non-linear changes in response to increasing concentration in which they first decreased then increased (DI), whereas others increased and then decreased (ID) (Fig. 2*A*, DI *vs*. ID).

The response from each glomerulus was segmented, and the fluorescence time course and odour response amplitudes ($\Delta F/F$) and corresponding z-scores were calculated as the largest difference in a 1200 ms moving window between the odour stimulation period and the baseline fluorescence. We quantified the concentration-response relationships in a population of glomerulus-odour pairings that included 736 individual glomeruli in 20 different preparations (36.8 ± 14.9 glomeruli per preparation, ranging 13–64). At least one odour was delivered to each preparation at five different concentrations, which included the odours methyl valerate ($n = 14$), isoamyl acetate ($n = 7$), benzaldehyde ($n = 7$), acetophenone ($n = 5$) and 2-phenylethanol ($n = 1$). The dataset includes 6495 glomerulus-odour pairings across all tested odours and concentrations (Fig. 2*B*). The fluorescence time course *versus* amplitude of all glomerulus-odour pairings illustrates that higher concentrations typically evoked stronger degrees of excitation and suppression in more glomeruli (Fig. 2*B*), though there are instances where this is not true, as discussed next.

We examined the relationship between concentration and response magnitude at the population level by plotting the $\Delta F/F$ evoked for each glomerulus-odour pairing for different odours (Fig. 2*C* and *D*). Sorting glomerular responses from smallest to largest for individual concentrations illustrates that relatively few glomeruli are activated at low concentrations, whereas the number of activated glomeruli and their overall response amplitude increased at higher concentrations (Fig. 2*C*). Sorting glomeruli by their response to the highest concentration more clearly visualizes concentration-response heterogeneity across the population (Fig. 2*D*). For many glomeruli the response to the highest concentration evoked the largest amplitude

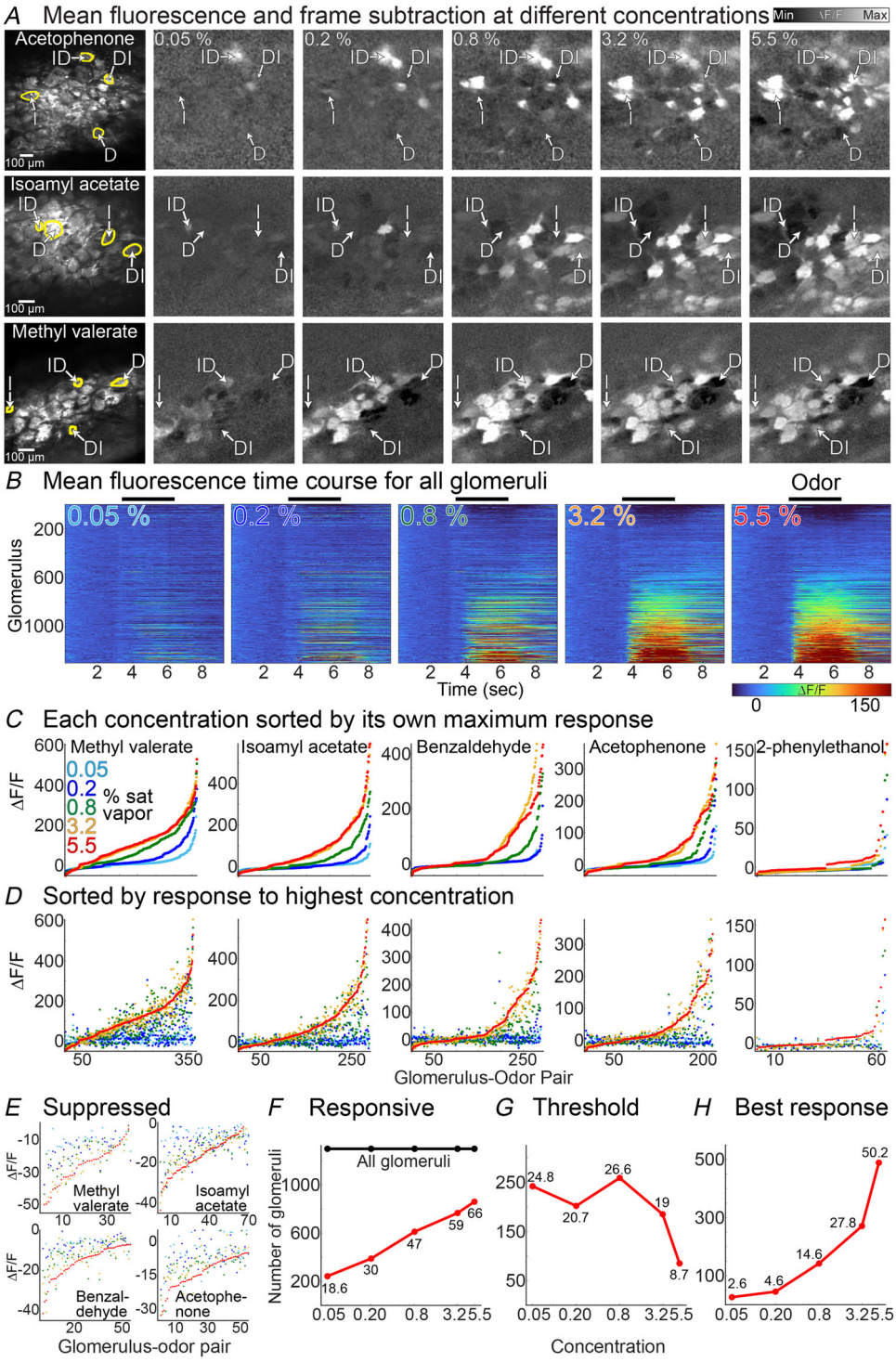

Figure 2. Concentration-response properties of MTC glomeruli
A, mean fluorescence (left subpanel) and frame subtractions illustrating mitral and tufted cell (MTC) activation at different concentrations in three preparations (rows). The intensity scale is fixed within each preparation. The arrows highlight glomeruli with increasing (I), decreasing (D), increasing–decreasing (ID) and decreasing–increasing (DI) concentration-response relationships. *B*, fluorescence time course from all glomerulus-odour pairings. The colour scale is fixed across the five concentrations. *C*, response to all glomeruli for each odour sorted by the maximum response to each concentration (colours). *D*, same arrangement as panel *C* except that glomeruli are sorted by the maximum response to the highest concentration. *E*, data from panel *D* cropped to visualize suppressed glomeruli. *F–H*, descriptive statistics. The numbers on each plot indicate the fraction of total glomeruli.

response (Fig. 2*D*, the red point is above the others), although other glomeruli responded with a submaximal response to the highest concentration (Fig. 2*D*, points of other colours are above red). For glomeruli with suppressed responses the highest concentration tended to evoke the strongest magnitude of suppression, but not always (Fig. 2*E*, data are cropped from panel *D*).

We quantified these observations using a statistical threshold in which significantly responsive glomeruli were defined as responding to the odour with a 5 SD change from the preodour frames. The number of significantly responsive glomeruli increased as a function of odour concentration (Fig. 2*F*). A similar analysis was used to define the lowest concentration that evoked a significant response for each glomerulus (the 'threshold' concentration) and the concentration that evoked the strongest response (the 'best' concentration). Of the responsive glomeruli approximately half had a threshold response of 0.8% of saturated vapour, whereas the remaining first responded to a lower or higher concentration (Fig. 2*G*). About half of the glomeruli responded most strongly to the highest tested concentration, whereas the remainder responded most strongly to a lower concentration (Fig. 2*H*). Increasing or decreasing the statistical threshold altered the number of 'responsive' glomeruli in the dataset but did not substantially change the mean threshold and best response of the glomeruli (not shown).

Examples of different MTC concentration-response categories

Representative examples from four different preparation-odour pairings illustrate that monotonic and non-monotonic glomerular concentration-response relationships were consistent across single trials and often present in the same field of view (Fig. 3*A*–*D*, all four glomeruli in each subpanel were simultaneously imaged in the same field of view).

Glomeruli categorized as I were present in 336 glomeruli and were defined as those that exhibited monotonically increasing response amplitudes from the lowest to the highest concentration, and which were never suppressed by the odour (Fig. 3*A*–*D*, first subpanel). I glomeruli could be well fit with the Hill equation with a mean Hill coefficient of 2.7 ± 1.2 (range 0.8–5.7, included 186 glomeruli in 24 preparation-odour pairings, the remainder were excluded due to poor fits, see Methods). We observed changes consistent with D in 125 glomeruli, which were defined as those that never increased in fluorescence in response to any odour-concentration pairing, but which exhibited a clear odour-locked decrease at the highest concentration. The mean $\Delta F/F$ and z-score of D glomeruli at the highest concentration was −21.6 ± 10.4 and 6.8 ± 4.6, respectively) (Fig. 3*A*–*D*, second subpanel). Glomeruli consistent with the ID response type were also present where higher concentrations drove increased response amplitudes up to a point at which further increases caused progressively smaller but still excited responses (Fig. 3*A*–*D*, third subpanel). ID concentration-response relationships were measured in 362 glomeruli and had a mean decrease in $\Delta F/F$ from the largest response amplitude to the response evoked at the highest concentration of 29.2 ± 31.9. Response types characteristic of DI were present in 92 glomeruli and were defined as having a suppressed response to at least one submaximum concentration and an excitatory response to the highest concentration (Fig. 3*A*–*D*, fourth subpanel). For DI glomeruli the mean ± SD $\Delta F/F$ and z-scores at the concentration with the largest-magnitude suppressed response were −13.7 ± 9.4 and 4.15 ± 2.2, respectively, and occurred most commonly at 0.2% (42/92) or 0.8% (35/92) of saturated vapour. Finally 34 glomeruli exhibited concentration-response relationships that included suppression but could not be clearly fit into any category (e.g. glomeruli that transitioned from strongly excited to suppressed, not shown). Thus of the 915 glomeruli that could be categorized, 37% were of type I, 14% were of type D, 10% were of type DI and 39% were of type ID.

Plots in which the concentration-response relationship of all glomeruli from each category were averaged together in each preparation-odour pairing illustrate that each response type was consistently present in nearly all preparations (Fig. 3*E*, left four subpanels, each line represents the average from one preparation). Averaging all responsive glomeruli together within the same field of view demonstrates that higher concentrations drive overall increasing levels of excitation across the glomerular population (Fig. 3*E*, all glomeruli, right-most subpanel), although this is often not true at the level of a single glomerulus. The correlation between concentration and mean response was significantly correlated for most individual preparations (0.67–0.97, mean of r = 0.87 ± 0.08, $P < 0.05$ in 18/32 preparation-odour pairings). Therefore excitation scales with changes in odour concentration in MTC glomeruli.

Different categories of MTC outputs are present when measured with different sensors

We tested whether the four general concentration-response categories were present in MTC glomeruli measured using two different genetically encoded calcium indicators, jRCaMP1b and jGCaMP8m (Fig. A2). Each response type was consistently present in all four preparations sampled across a large concentration range in four different odours (Fig. A3*A* and *B*, two preparations tested for each sensor). These results suggest that the presence of diverse concentration-response

relationships is unlikely to be the consequence of sensor properties specific to GCaMP6f.

MTC response categories are glomerulus- and odour-specific

Our model indicates that different linear and non-linear MTC concentration-response relationships are due to the specific combination of the Hill coefficient and half-activation value of the corresponding ORNs (Fig. 1*E*). One prediction of this is that the response category assigned to each glomerulus should be odour-specific. We tested this in a subset of preparations in which responses were measured to at least two different odours (N = 479 glomerulus-odour pairings in 15 preparation-odour pairings in six different mouse preparations; between two and four odours were tested per preparation). Activity maps ($\Delta F/F$) illustrate that response patterns were

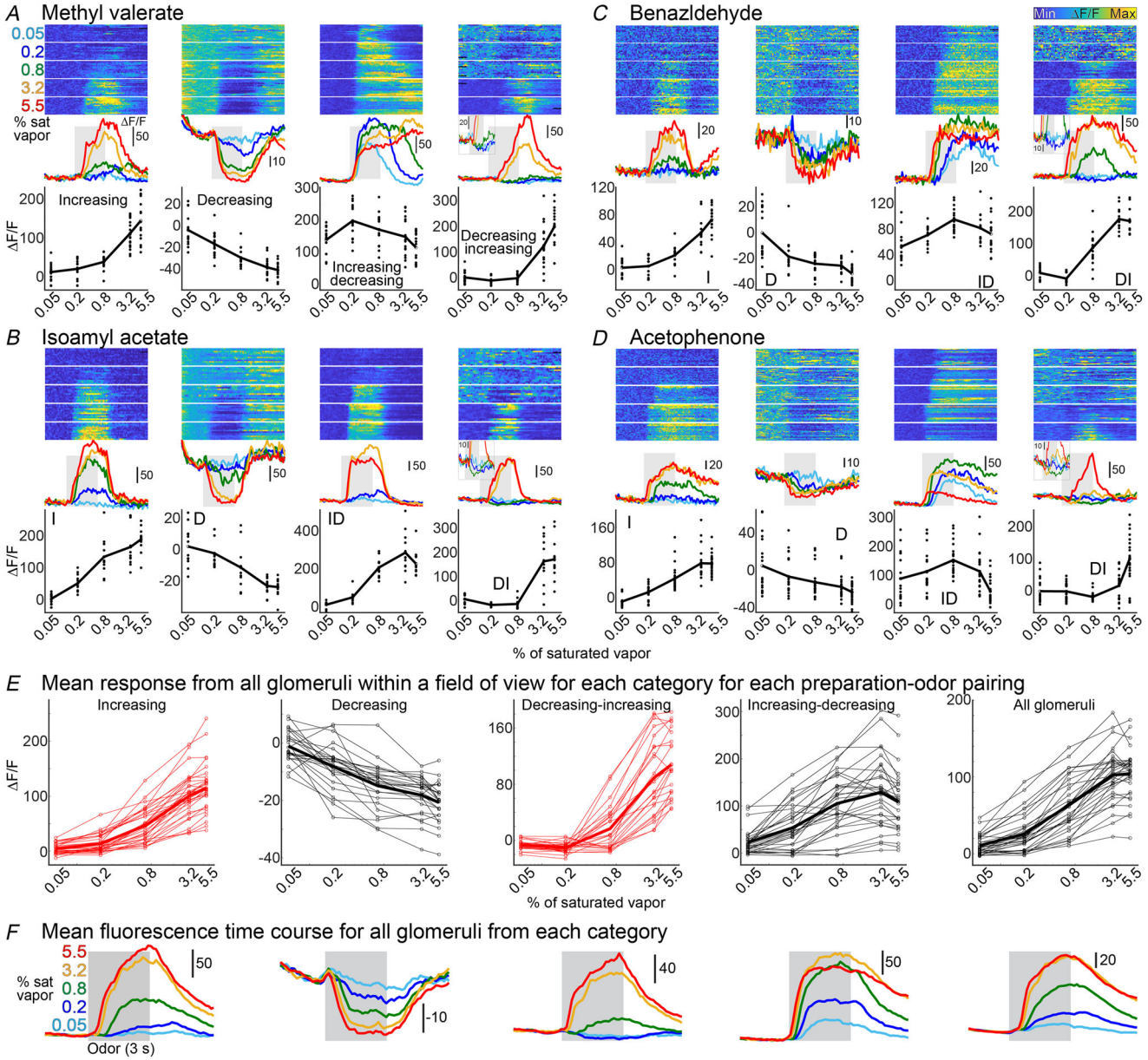

Figure 3. Different MTC glomerular response types
A–D, single trials (top), mean fluorescence time course (middle) and concentration-response relationships, with points indicating the response amplitudes from the single trials for four different preparations. *E*, mean concentration-response relationships for each preparation-odour pairing for each response type (first four subpanels) and across all glomeruli in each field of view (right-most subpanel). *F*, mean fluorescence time course from all glomeruli in each category.

concentration-dependent and odour-specific (Fig. 4*A*). The different response categories of each glomerulus were identified using the previously described criteria and were mapped using different colours. For each preparation the same glomerulus could exhibit the same kind of response or entirely different categorical responses (Fig. 4*B*). The effect of odour changes from each category to another is illustrated as a two-dimensional histogram and a network graph (Fig. 4*C* and *D*). Changing the odour resulted in the same response category in 38.8% of glomeruli, with the most common occurrence being NR glomeruli remaining as NR (15.6%) (Fig. 4*C* and *D*, NR *vs*. NR). The remainder of the glomeruli transitioned categories, with the most common outcome being that NR transitioned to I (12.5%) (Fig. 4*C* and *D*, NR *vs*. I). Therefore the proportions of MTC categories observed across the population are a function of odour-driven variability.

The response magnitude of decreasing MTC glomeruli scales proportionally with mean excitation across all glomeruli

Another prediction from our model is that higher levels of excitation should evoke increasing levels of inhibition (Fig. 1*B* and *C*, dotted line). We tested this prediction by comparing the mean of all excited glomeruli within a field of view against the mean of all D glomeruli within a field of view. The response to all concentrations was included for each glomerulus if it responded at any concentration. In four exemplar preparation-odour pairings there was a strong and sometimes statistically significant relationship between normalized excitation and suppression (Fig. 5*A*–*C*, the number of excited and suppressed glomeruli in each preparation-odour pairing is indicated in panel *B*).

The relationship between excitation and suppression was significantly correlated in 18 out of the 27 preparation-odour pairings included in the analysis (Fig. 5*D*, mean $r = 0.89 \pm 0.07$, statistically significant preparations are indicated in red) and when combining all preparation-odour pairings together (Fig. 5*E*, $r = -0.67$, $P < 0.001$). Additionally the individual points from all preparations were binned together, the values of which were fit to a sigmoid (Fig. 5*E*, thick black line and circles and the dashed line; different fitting parameters yielded similar fits). Although there was variance in the mean values, a clear sigmoidal decline was accounted for a substantial amount of the variance (Fig. 5*E*). Therefore suppression scales with increasing levels of excitation in subsets of MTC glomeruli.

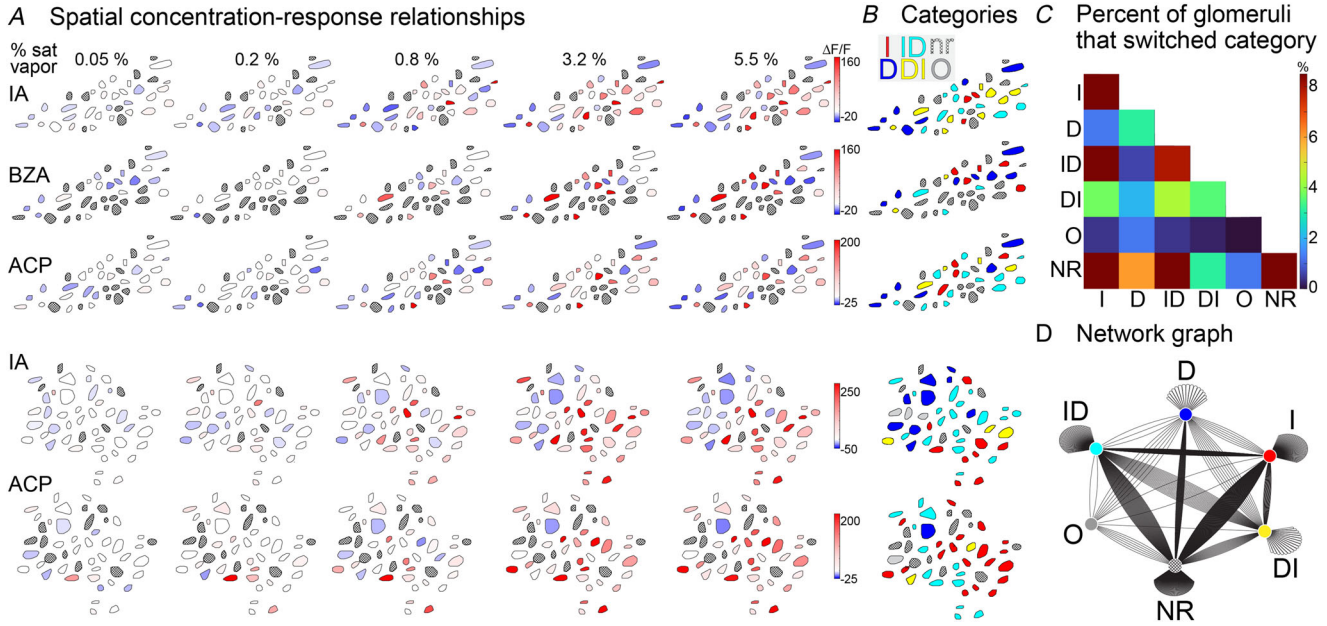

Figure 4. MTC glomerular response types are odor-specific
A, maps of glomerular odour responses ($\Delta F/F$) in different preparations in response to different odours. The colour scale is fixed across all concentrations for each preparation-odour pairing. Glomeruli that do not respond to any concentration are indicated with a hatched overlay. *B*, maps of glomerular response categories: I, increasing; D, decreasing; DI, decreasing then increasing; ID, increasing then decreasing; nr, non-responsive; O, other type not clearly associated with any category. IA, isoamyl acetate; BZA, benzaldehyde; ACP, acetophenone; MV, methyl valerate. *C*, a histogram and network graph illustrate how changing the odour changed the proportions of each response type. *D*, network graph illustrating transitions between categories as a function of odour change.

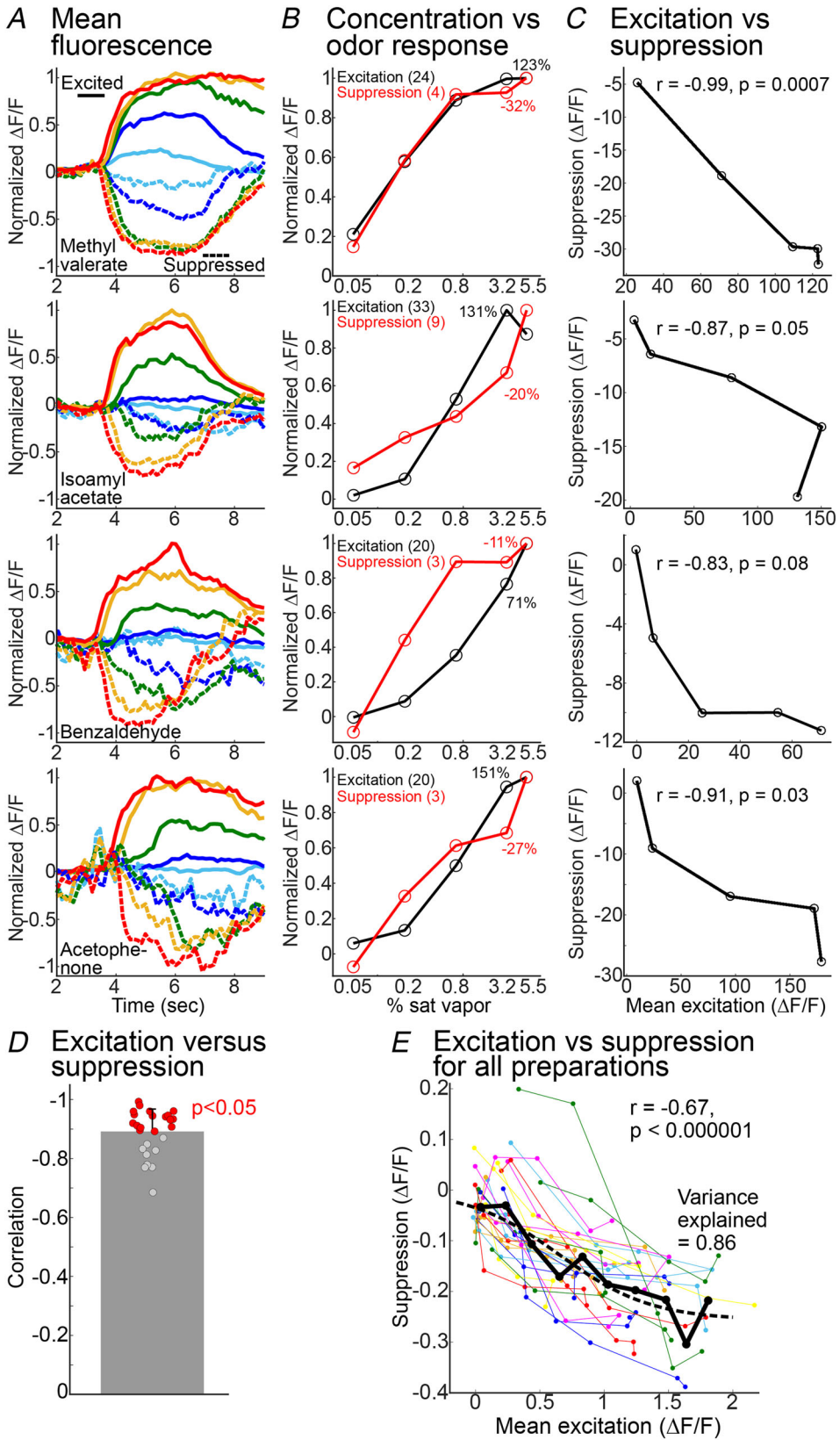

Figure 5. The magnitude of excited and suppressive MTC odor responses scales with increasing concentration

A–C, mean fluorescence time course of excited (solid traces) and suppressed (dashed traces) glomeruli (*A*), concentration *versus* normalized Δ*F*/*F* (*B*) and excitation *versus* suppression (*C*) for four preparations. The number

of glomeruli averaged together and the maximum $\Delta F/F$ values are indicated in subpanel *B*. *D*, correlation between excitation and suppression for each preparation. *E*, mean excitation *versus* suppression for all preparations. Each individual point is the average of all the excited and suppressed glomeruli within a field of view for one concentration-odour pairing. Measurements from the same preparation-odour pairing are connected with a line. The individual points are binned (solid black line and black circles) and fit to a sigmoid (dashed line).

The concentration-response relationships of increasing–decreasing MTC glomeruli are heterogeneous and have more sensitive odour responses

Our model predicts that ID responses reflect input from higher-affinity ORNs due to receptor saturation, and that differences in the balance of excitation and inhibition should yield differences in the degree of non-monotonicity (Fig. 1*D*–*F*). We quantified the heterogeneity of ID responses using an MI which assigns monotonic glomeruli (i.e. I) a value of 0, whereas non-monotonic glomeruli (e.g. ID) are assigned increasingly negative values depending on the magnitude of the decrease (Escabí et al., 2007; Higgins et al., 2008).

Concentration-response relationships from simultaneously imaged glomeruli in two different preparations illustrate different I and ID responses (Fig. 6*A* and *B*). We quantified the MI for all responsive glomerulus-odour pairings except for exclusively suppressed glomeruli (D) because they are assigned a strongly negative MI value (Fig. 6*C*). Glomeruli binned into different MI ranges illustrate the heterogeneity of ID responses across the MTC population (Fig. 6*C*). Within the population of non-suppressed MTC glomeruli 53% exhibited some degree of non-monotonicity (Fig. 6*D*).

The MI incorporates response variability at each concentration to assign a value and therefore provides an unbiased approach to defining the two categories (see eqn (6)). Additionally the MI value was significantly correlated with the linear slope of the concentration-response relationship ($r = 0.6$, $P < 0.0001$). Therefore our metrics accurately capture the differences between monotonic and non-monotonic glomeruli.

We quantified the sensitivity of each MTC glomerulus with piecewise linear interpolation of each concentration-response relationship, which was used to quantify the concentration evoking the half-maximum response (Fig. 6*A* and *B*, dashed vertical lines). In this analysis glomeruli in which the response to the lowest concentration was greater than the half-maximum were assigned a value of 0.05% (e.g. Fig. 6*B*, roi 9). ID glomeruli with more negative MI values tended to have lower half-maximum values in our exemplar preparations (Fig. 6*A* and *B*, vertical lines) and across the population (Fig. 6*E*, left panel, 324 glomerulus-odour pairings across 17 preparation-odour pairings). This relationship was significantly correlated ($r = 0.47$, $P < 0.0001$), and the half-maximum value of I glomeruli was significantly higher than ID glomeruli (Fig. 6*E*, right panel, $P \leq 0.00046$ for all comparisons with MI = 0). Thus MTC glomeruli with ID responses tend to reach their half-maximum response at lower concentrations than those exhibiting monotonically increasing relationships with odour concentration.

An approach to measure the OB input–output transformation using dual-colour two-photon imaging

The result that MTC glomeruli with smaller half-maximum values tend to be more non-monotonic is consistent with the model predictions (Fig. 6*E*). However a stronger and more direct test would involve systematically relating odour sensitivity to glomerular response profiles by functionally imaging ORN and MTC glomeruli. Therefore we generated a transgenic mouse in which GCaMP6s was expressed in the ORNs, and jRCaMP1b was selectively expressed in MTCs and their apical dendrites innervating the glomerular layer (Fig. 7*A* and *B*). *In vivo* experiments were performed in awake mice in which the dorsal OB was selectively illuminated with 920 nm to measure GCaMP fluorescence and 1100 nm to measure jRCaMP1b fluorescence (Fig. 7*C*, top row illustrates the mean fluorescence from two different preparations). In an abundance of caution we performed all measurements of ORNs and MTCs in separate imaging trials that were illuminated with 920 or 1100 nm, respectively, due to the relatively long emission tail present for GCaMP (Akerboom et al., 2012). Imaging trials carried out at 920 and 1100 nm are hereafter referred to as ORN and MTC measurements, respectively. Odour responses were measured in four different mouse preparations to methyl valerate, isoamyl acetate, acetophenone and methyl salicylate delivered at six liquid dilutions ranging from 0.002% to 10% and air (a total of eight preparation-odour pairings). A frame-subtraction analysis revealed that odours evoked changes in glomerular-sized regions of interest in both the ORN and MTC measurements (Fig. 7*C*, bottom row).

Non-monotonic increasing–decreasing MTC glomerular outputs originate from more-sensitive ORN inputs

The ORN and MTC odour response time course and corresponding concentration-response relationships

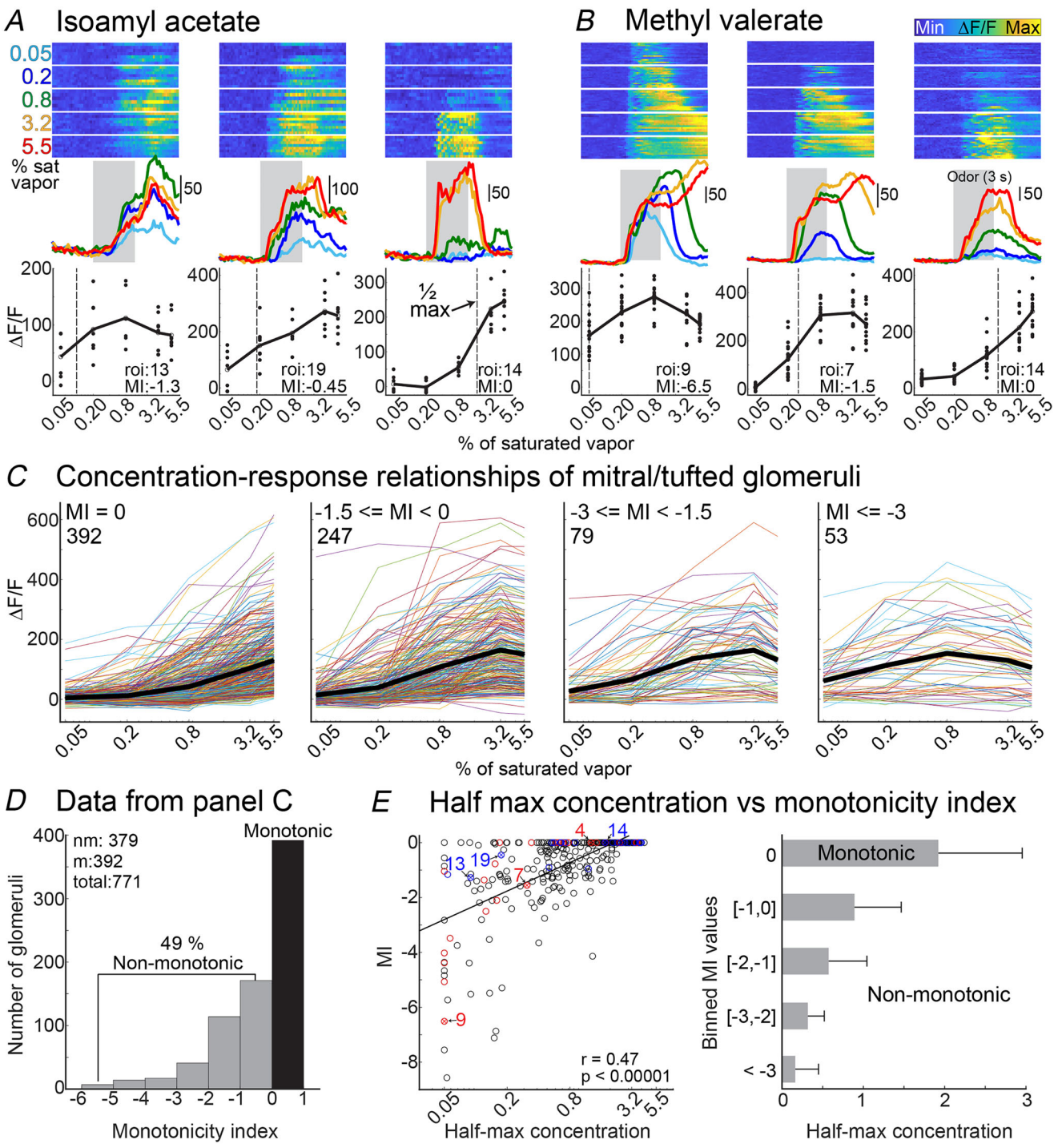

Figure 6. Non-monotonic ID MTC glomeruli are common and heterogeneous
A and *B*, single trials (top row), mean fluorescence time course (middle) and mean concentration-response relationships (bottom) for three mitral and tufted cell (MTC) glomeruli in two preparation-odour pairings. The vertical lines in the bottom subpanel of *A* and *B* indicate the half-maximum concentration. *C*, concentration-response relationships for all responsive MTC glomeruli from all preparations binned by their monotonicity index (MI), with the mean indicated with a black line. The number of glomeruli in each bin is in the top left of each panel. *D*, histogram of MI values from panel *C*. *E*, the relationship between half-maximum concentration and MI. The coloured circles in the left subpanel indicate measurements from the preparations in panels *A* and *B*.

are illustrated for three glomeruli from two different preparation-odour pairings (Fig. 8*A* and *B*). The most sensitive ORN glomeruli often had correspondingly non-monotonic MTC outputs with small and sometimes negative slopes (Fig. 8*A* and *B*, left-most panels). We quantified the affinity of each ORN glomerulus by measuring the half-maximum value of the concentration-response relationship (e.g. Fig. 8*A*, vertical lines in the top row) and the steepness of each MTC glomerulus by measuring the linear slope of the concentration-response relationship. The relationship between ORN affinity and MTC slope is illustrated

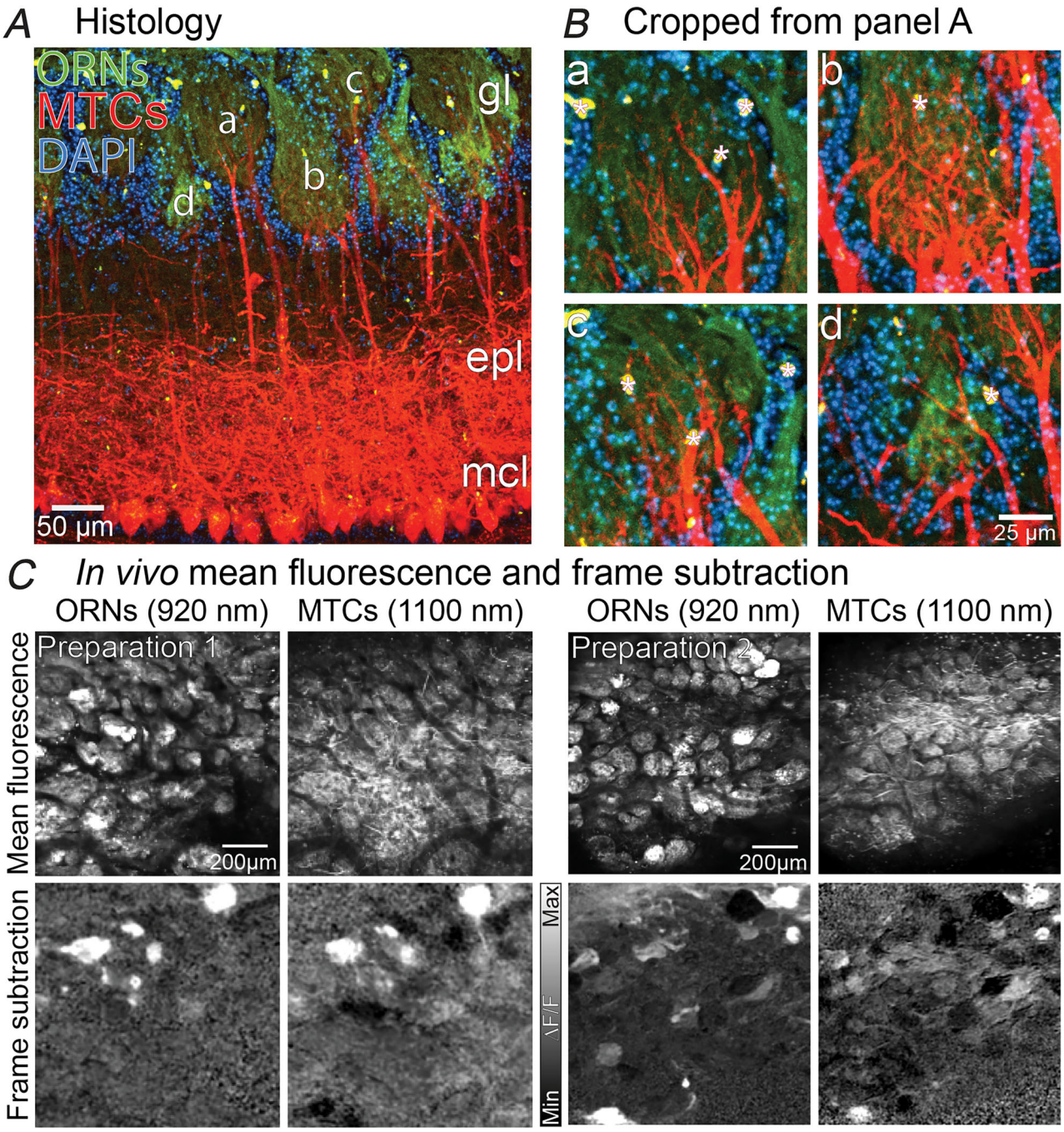

Figure 7. Labeling ORNs and MTCs with spectrally distinct Ca^{2+} sensors indicato
A and *B*, histology from a transgenic mouse expressing GCaMP6s in the olfactory receptor neurons (ORNs) and jRCaMP1b in the mitral and tufted cells (MTCs). The bright yellow spots indicated with asterisks are lipofuscin autofluorescence. *C*, mean fluorescence and frame subtraction odour responses from the ORNs (imaged using 920 nm excitation) and MTCs (imaged using 1100 nm excitation) in two mouse preparations.

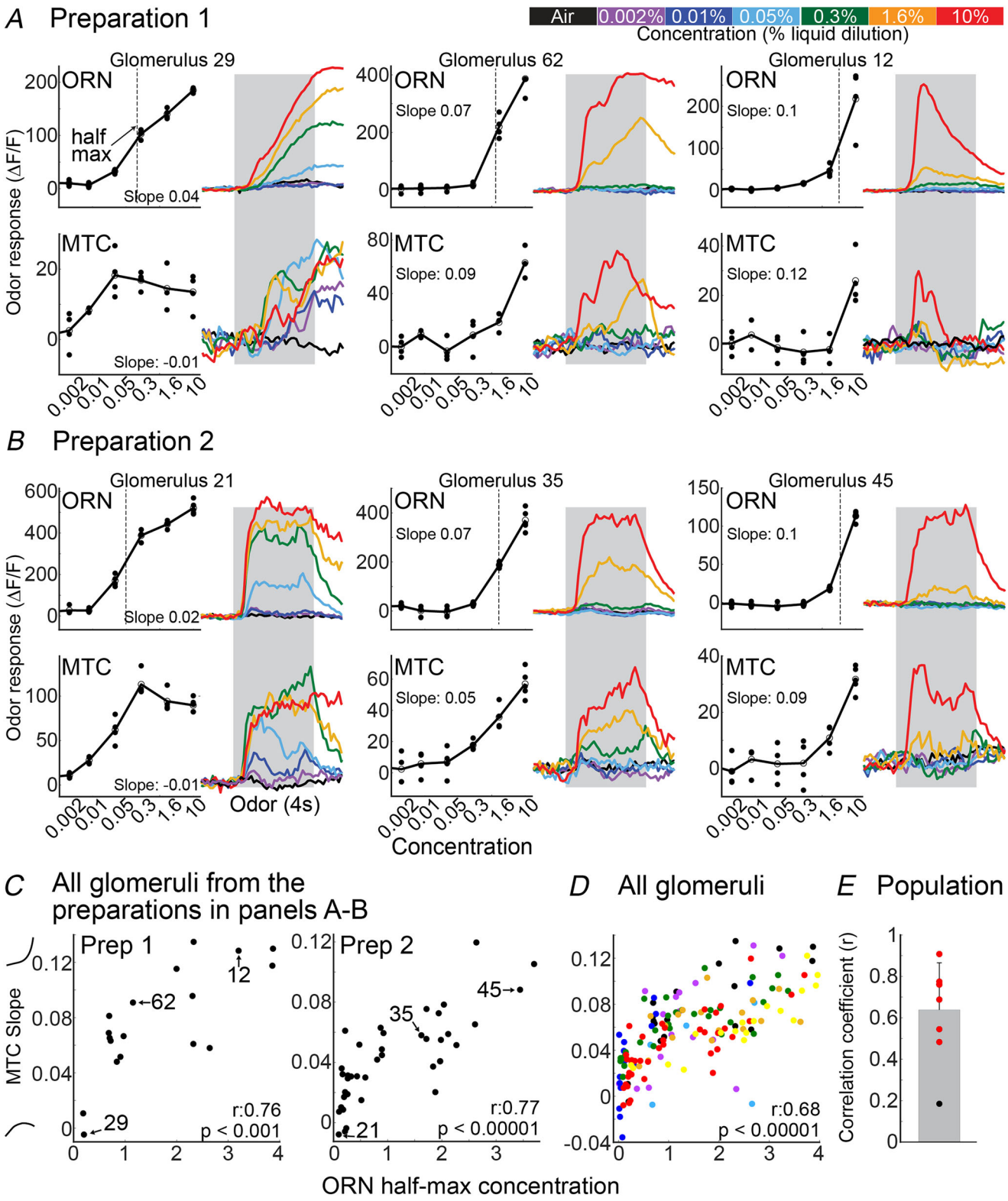

Figure 8. Non-monotonic MTC glomeruli originate from sensitive ORN inputs
A and *B*, input–output measurements from three glomeruli from two different mouse preparations. The glomeruli are sorted from lowest (most sensitive) to highest (least sensitive) half-maximum concentration values. *C* and *D*, the correlation between olfactory receptor neuron (ORN) half-maximum and the slope of the mitral and tufted cell (MTC) concentration-response relationship for glomeruli in the preparations in panels *A* and *B* (*C*), and for all glomeruli in eight preparation-odour pairings (*D*). *E*, correlation coefficient of all eight preparation-odour pairings. Red circles indicate a preparation with a significant correlation.

for the two preparations in panels *A* and *B* in Fig. 8*C* and was significantly correlated when combining all tested glomeruli from four preparation-odour pairings (Fig. 8*D*, $N = 163$ glomeruli, colour indicates glomeruli from different preparation-odour pairings). Finally this relationship was significantly correlated in seven to eight preparation-odour pairings in the dataset (Fig. 8*E*).

Decreasing MTC glomeruli originate from lower-sensitivity ORN inputs

Another prediction is that D MTC glomeruli are the consequence of input from ORNs with low sensitivity to an odour ORNs with more sigmoidal concentration-response relationships, in which the rising levels of lateral inhibition exceed the feed-forward ORN excitation. We tested this prediction by measuring the input–output relationship of MTC glomeruli that were clearly suppressed by the odour at the highest concentration (e.g. Fig. 9*A*, output). Our dataset included 63 MTC glomeruli from five preparation-odour pairings (three different animals) that were suppressed by the odour in response to the highest tested concentration, with a mean *z*-score change in 6 ± 2.9 from baseline (Fig. 9*A*, output). Of the MTC glomeruli with suppressed odour responses 35/63 had an ORN odour responsive to at least one concentration with a minimum change of 5 SDs above baseline (e.g. Fig. 9*A*, input). The ORN inputs to the D MTC glomeruli had significantly larger half-maximum concentrations than the ORN input to non-D glomeruli when comparing individual glomeruli (D: 3.5 ± 0.9, $N = 35$; non-D: 1.6 ± 1.1, $N = 133$ glomeruli, $P < 0.0001$), or when averaging glomeruli within each preparation-odour pairing (D: 3.7 ± 1.2, $N = 5$; non-D: 1.7 ± 0.5, $N = 5$, $P < 0.0079$) (Fig. 9*B*). Interestingly the remaining 28/63 D MTC glomeruli originated from ORN inputs that were non-responsive to the same odour (Fig. 9*C*, compare response of MTC and ORN to isoamyl acetate). In the subset of the non-responsive inputs that were tested to multiple odours most could be activated by another odour (10/13) (Fig. 9*C*, compare response of ORN to isoamyl acetate and acetophenone or methyl valerate). This indicates that the lack of an ORN response to isoamyl acetate was not due to poor labelling or other methodological explanations. Together these results are consistent with the idea that D glomeruli of MTC are primarily innervated by lower affinity ORN glomeruli, which is consistent with the model predictions.

The presence of both monotonic and non-monotonic responses broaden MTC state space

One advantage of having four distinct response types to an odour over a range of concentrations is that it provides a broader range of coverage of the MTC state space. As a simple example we consider only three glomeruli, with output MTC_1, MTC_2 and MTC_3. The response amplitude of each to an odour at a given concentration would be a point in the MTC_1-MTC_2-MTC_3 state space, and the response to that odour over a range of concentrations would be a set of points that can be thought of as a directed curve, or trajectory, in that space (Fig. 10). The neural coding of an odour across concentrations in the OB would then be a trajectory in the MTC state space. The response to a second odour over a similar range of concentrations would produce a different trajectory. In both cases the trajectory should be considered a cloud of points that reflect variations in the fluctuations of molecular components present in natural odour stimuli (whether due to differences in chemistry or environmental interactions). An animal would learn to recognize an odour in a concentration-invariant manner as the population activation along that trajectory based on experience. To illustrate how different response types impact the coverage of the MTC state space we show a collection of trajectories all having an I response to an odour (black curves in Fig. 10) and an equal number having a mix of monotonic and non-monotonic response types (red curves in Fig. 10). Each trajectory is based on calcium measurements from three glomeruli. When all responses are of the I type they cover only a small region of the state space. In contrast when non-monotonic responses are included the coverage is much more extensive. The greater coverage makes it easier to discriminate one odour from another, and even though the dimension of the actual MTC state space is much larger than 3 (equal to the number of different receptor types) it is still advantageous to increase the coverage of that space, as is done by having different response types to odours.

Discussion

Here we identify a novel neural transformation in the OB in which monotonic sensory inputs are transformed into a diverse array of MTC outputs. By combining a predictive model with single and dual-colour *in vivo* two-photon Ca^{2+} imaging we demonstrate that the MTC CRFs are actively computed by the OB network rather than being inherited from the periphery. Increasing odour concentration recruited a range of non-monotonic and suppressed responses that were absent from their corresponding ORN inputs. Importantly the MTC outputs were not random but, instead, were predictable based on the sensitivity of their ORN inputs. Our modelling results provide a mechanistic basis for this transformation, distinguishing between the two kinds of non-monotonic responses present in our empirical dataset based on the relative contributions of intraglomerular and interglomerular inhibition. These

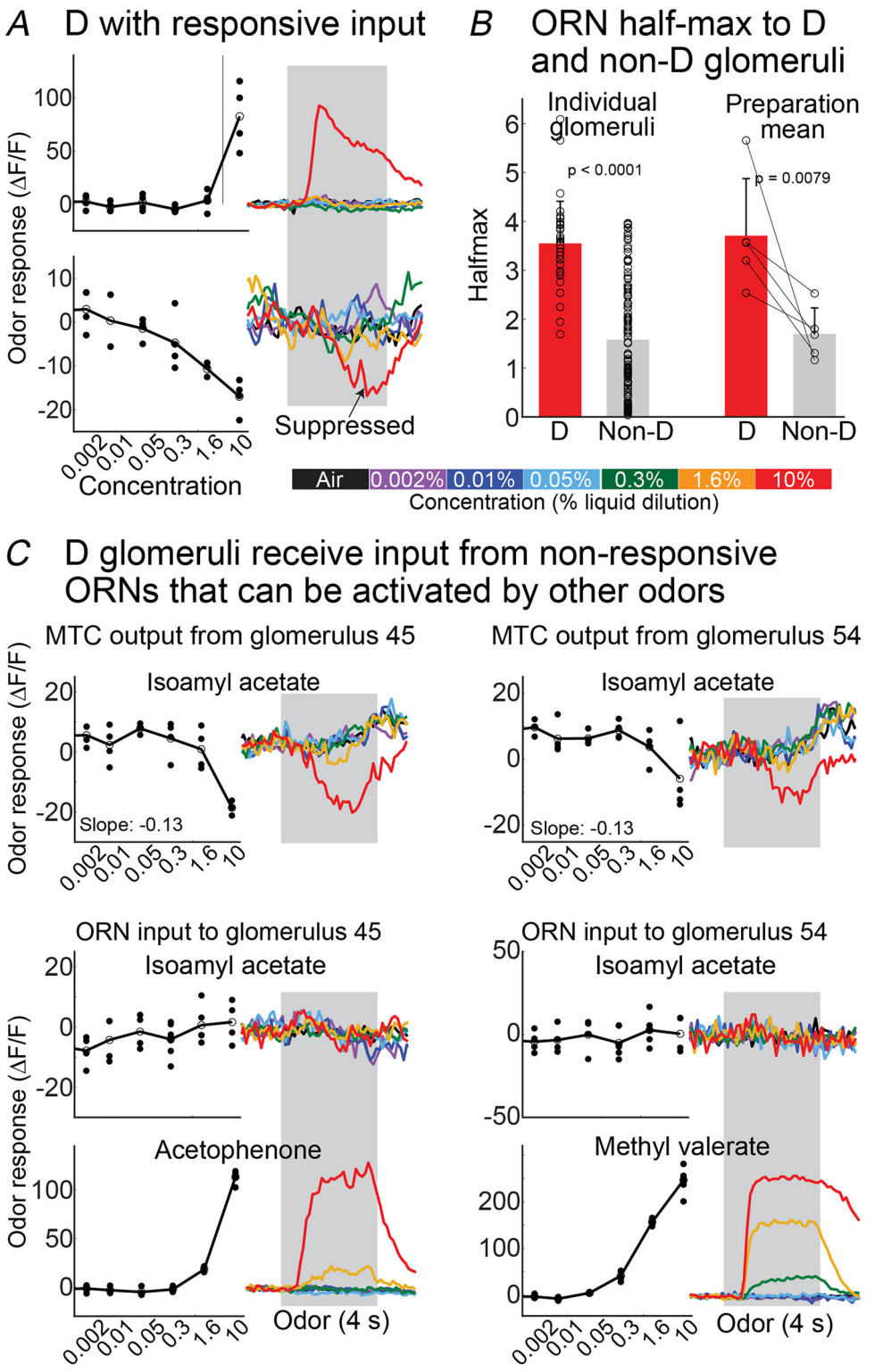

Figure 9. MTC D glomeruli originate from lower sensitivity ORN inputs
A, a mitral and tufted cell (MTC) glomerulus with a D concentration-response relationship that receives input from olfactory receptor neuron (ORN) with a high half-maximum concentration. *B*, mean half-maximum value of all individual ORN glomeruli with D responses, and for all non-D glomeruli in the same preparation-odour pairings (left) and the mean for each preparation (right). *C*, two MTC glomeruli with D responses received ORN input that was not responsive to the same odour (isoamyl acetate) but could be activated by other odours (bottom; acetophenone and methyl valerate).

theoretical results were supported by the observation that the magnitude of suppressed responses scales with increasing concentration. This process broadens MTC odour state space, providing a mechanistic basis for how the olfactory system maintains concentration-invariant odour perception and facilitates odour discrimination.

Rationale for our modelling choices

A fundamental assumption of the model is that the response function of periglomerular cells (PGCs) that provide local inhibition is left-shifted relative to that of mitral cells and has a lower saturating level (Fig. 1*B*). This provides local half-hat coding, so that weaker input signals are suppressed while stronger ones get through (Cleland, 2010; Cleland & Sethupathy, 2006). Another assumption is that there is lateral inhibition that increases with the odour concentration (e.g. the dashed curve in Fig. 1*C*). Without this lateral inhibition the model produces only two response types: I and DI (Fig. A1*B*). If the half-hat assumption is incorrect, and local interneurons are activated at higher-odour concentrations than the mitral cells, then ID mitral cell responses could be produced with local inhibition alone, but in that case DI responses would not be produced through local inhibition. The most parsimonious hypothesis is then that the PGC activation function is left-shifted, and primarily responsible for the suppression in DI responses, whereas lateral inhibition is responsible for the suppression at higher-odour concentrations and thereby yielding ID responses.

Our model implements interglomerular lateral inhibition by means of divisive normalization, a well-established mechanism for implementing gain control and contrast enhancement in sensory systems (Carandini & Heeger, 2011). Divisive mechanisms have been observed or proposed in multiple sensory modalities, including the olfactory, auditory and

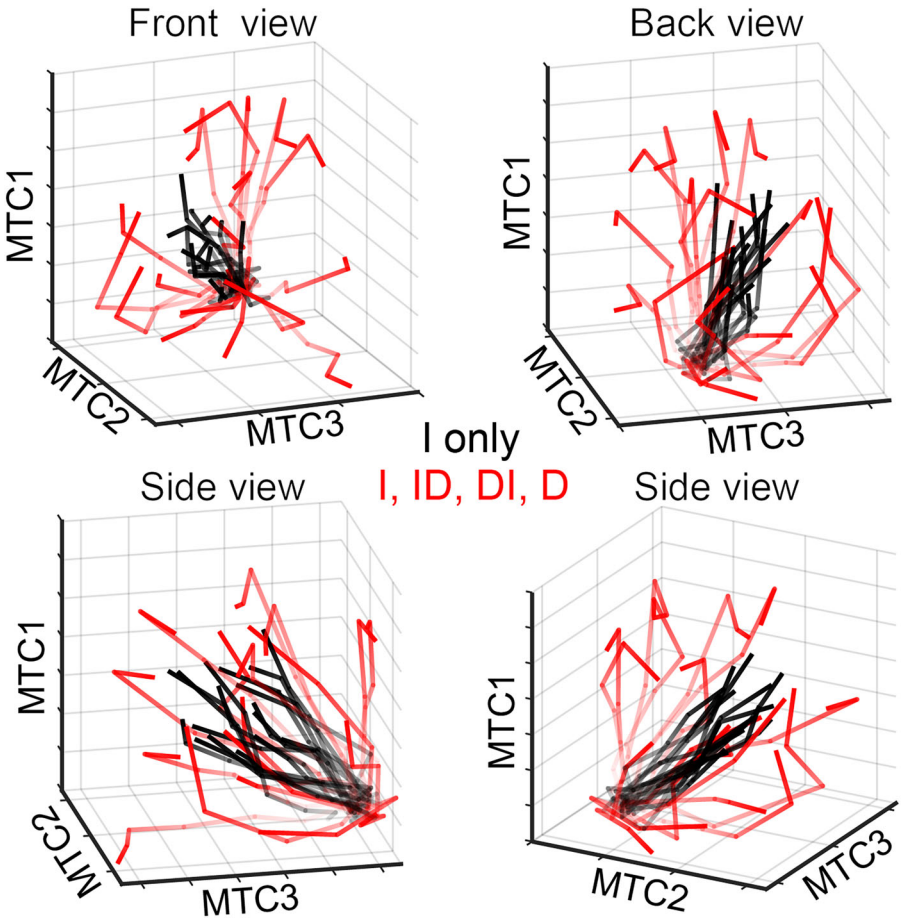

Figure 10. Model of how the different MTC response types influence odour coding
Each line in this model illustrates the response of three MTC glomeruli to a single odour across concentration changes. Concentration changes are represented as the changing transparency of each line. MTC glomeruli with only increasing responses tended to cluster together in space (black lines). In contrast MTC glomeruli with different response categories had response trajectories that diverged from one another (red lines). Each panel illustrates the projections from a different angle.

somatosensory systems (Carandini & Heeger, 2011; Olsen et al., 2010; Rabinowitz et al., 2011). In the olfactory system support for the existence of this mechanism has been shown anatomically and functionally, although the extent of interglomerular inhibitory coupling remains unclear (Aungst et al., 2003; Banerjee et al., 2015; Cleland et al., 2007; Economo et al., 2016; Olsen et al., 2010; Shen et al., 2025; Storace & Cohen, 2017; Zavitz et al., 2020; Zhu et al., 2013). We assumed that the lateral inhibition of the input to a glomerulus was from a randomly selected subpopulation of the glomeruli. Increasing the size of the normalizing subpopulation sharpened the boundaries between the different response types (Fig. 1*E* and *F*). However the model can also be further developed to consider the impact of different interglomerular inhibitory network structures, including those with distinct spatial or functional clustering (Zavitz et al., 2020).

The general effect of lateral inhibition in our model requires that it occur presynaptically to MTCs. Therefore lateral inhibition in our model reflects a combination of different forms of network activity, including ORN presynaptic inhibition and multisynaptic pathways presynaptic to MTCs, such as granule cell-mediated lateral inhibition and feedback from other brain areas (Banerjee et al., 2015; Kapoor et al., 2016; Otazu et al., 2015; Petzold et al., 2009; Rothermel & Wachowiak, 2014; Vucinic et al., 2006; Zak et al., 2024).

Comparison with previous studies

Our study provides key insights that advance beyond previous studies that measured concentration-response relationships from individual MTCs or their glomerular tufts (Banerjee et al., 2015; Economo et al., 2016; Niessing & Friedrich, 2010; Yamada et al., 2017). We used dual-colour two-photon Ca^{2+} imaging from the ORN axon terminals and the MTC apical dendrites innervating the same glomeruli to demonstrate that these non-monotonic dynamics are computed via a transformation across the OB network, as opposed to being inherited from the periphery. Furthermore our dual-colour approach allowed us to link MTC response types to specific ORN input characteristics. Specifically we show that non-monotonic and suppressed MTC glomerular responses are predictable based on ORN sensitivity. These insights fundamentally advance our previous OB input–output measurements, which used epifluorescence imaging, a method that lacked the spatial resolution required to resolve these distinct neural transformations (Storace & Cohen, 2017).

Current models of how inhibitory circuits are shaped by excitation propose that inhibition either increases broadly or selectively across the glomerular population in a manner that scales with the magnitude of excitatory input (Banerjee et al., 2015; Cleland et al., 2007; Economo et al., 2016; Zavitz et al., 2020). Our theoretical and experimental results suggest that ID glomeruli reflect processing that occurs within the OB as higher-sensitivity ORNs compress near the upper limit of their dynamic range, allowing rising lateral inhibition to outweigh their excitatory drive. Indeed ID responses have rarely been described at the level of the input to the OB (Bozza et al., 2004; Inagaki et al., 2020; Lecoq et al., 2009; Platisa et al., 2022; Storace & Cohen, 2017; Wachowiak & Cohen, 2001; Zak et al., 2020). Additionally we find that suppression and overall excitation are significantly correlated, which is consistent with reports of interneurons that mediate lateral connectivity exhibiting activity that scales with increasing odour concentrations (Banerjee et al., 2015; Storace et al., 2019; Zhu et al., 2013).

Our results differ somewhat from recent experimental reports describing different proportions of non-monotonic MTC glomeruli (28.7% whereas we found 49%), and that the amount of excitation in MTC glomeruli was weakly predictive of the magnitude of suppression (Economo et al., 2016; Zavitz et al., 2020). These differences may be due to methodological differences, including the anaesthetic state of the animal and the fact that all glomeruli in our dataset were tested at each concentration.

ORNs can undergo rapid adaptation in response to prolonged or high-frequency sampling of an odour stimulus (Duchamp-Viret et al., 2000; Lecoq et al., 2009; Verhagen et al., 2007). However we did not observe rapid adaptation in the ORN input to MTC glomeruli with ID response types (Fig. 8*A* and *B*), and ID MTC glomeruli often remained elevated throughout the odour presentation (e.g. Figs 3*A*,*B* and 6*A*,*B*). However because we did not measure the ORN input to all glomeruli in our dataset we cannot rule out the possible contribution of ORN adaptation in some non-monotonic responses.

Methodological considerations

Ca^{2+} indicators provide an indirect report of neural activity, which is shaped by distinct biophysical properties, including affinity, slope and binding dynamics (Badura et al., 2014; Chen et al., 2013; Dana et al., 2016; Helassa et al., 2016; Zhang et al., 2023). Importantly Ca^{2+} indicators with non-linear Hill coefficients still exhibit a strong relationship between spiking activity and changes in fluorescence (Akerboom et al., 2012; Chen et al., 2013; Dana et al., 2016; Kato et al., 2012; Tian et al., 2009; Wachowiak et al., 2013; Zhang et al., 2023). However the ability to detect neural activity across a large range of spiking is ultimately limited by the dynamic range of the protein sensor itself (Wachowiak et al., 2013). Because MTCs have relatively high spontaneous firing

rates the ability of GECIs to report the full range of their spiking activity may be limited (Rinberg et al., 2006). The observation that we measured ID and DI responses using three different Ca^{2+} indicators suggests that they cannot be easily explained by limitations of the indicator.

Although MTC glomerular Ca^{2+} signals do not exclusively reflect somatic spiking activity, mitral cell action potentials initiated at the soma backpropagate into primary dendrites which evoke corresponding Ca^{2+} transients that are substantially larger than those evoked by presynaptic input (Bischofberger & Jonas, 1997; Charpak et al., 2001; Chen et al., 1997; Chen et al., 2002; Christie & Westbrook, 2003; Debarbieux et al., 2003; Djurisic et al., 2004; Kato et al., 2012; Wachowiak et al., 2013; Zhou et al., 2006).

The Tbx21-cre transgenic strain used in our study drives expression in both MTCs (Mitsui et al., 2011; Storace & Cohen, 2021), which can have distinct concentration-response relationships and are embedded differently into the glomerular network (Chae et al., 2022; Fukunaga et al., 2012; Igarashi et al., 2012; Kikuta et al., 2013; Nagayama et al., 2004; Shen et al., 2025). Therefore our two-photon imaging from the apical dendrites of MTCs innervating glomeruli necessarily includes signals from both cell types. Future experiments incorporating more selective targeting to mitral *versus* tufted cells are needed to clarify their distinct functional role(s) in glomerular signalling (Koldaeva et al., 2021; Rothermel et al., 2013; Wachowiak et al., 2013).

Although DI response types could be detected at our second-lowest concentration, the non-monotonic component of ID glomeruli and many detectable D responses typically emerged at higher concentrations that an animal is unlikely to experience in its natural environment (Wachowiak et al., 2025). We propose that the ID responses we describe are more likely to occur in more natural contexts, which can contain multiple odour sources that will activate multiple glomeruli and, therefore, higher levels of lateral inhibition.

Functional relevance of non-monotonic concentration-response relationships

Neurons with non-monotonic intensity relationships have been described in the auditory system and exhibit unique characteristics, such as being sensitive to behavioural training and exhibiting adaptive properties (Higgins et al., 2010; Polley et al., 2004; Polley et al., 2006; Polley et al., 2007; Sutter & Loftus, 2003; Watkins & Barbour, 2008; Wehr & Zador, 2003). Although our model indicates that these glomeruli are due to the interplay between intra- and interglomerular inhibition, it remains to be tested whether these strongly suppressed glomeruli are functionally unique.

Additional considerations

More comprehensive measurements of the input–output relationship before and after selective manipulation of different cell types or with more precise control over the input stimulus will allow us to test additional predictions of our model (Banerjee et al., 2015; Braubach et al., 2018; Burton et al., 2022; Smear et al., 2013). For example these approaches can be used to test the hypotheses that DI responses are due to intraglomerular processing, whereas ID responses require interglomerular processing, and that the Hill coefficient plays an important role in the transformation of each glomerulus.

Although we focus on the amplitude of the Ca^{2+} response, timing is also important for the neural coding of odour (Ackels et al., 2021; Chong et al., 2020; Shusterman et al., 2011; Smear et al., 2011). Indeed the 'primacy coding' scheme hypothesizes that only those receptors that act earliest are responsible for the neural coding of an odour (Wilson et al., 2017). In this model whether the MTC response is monotonic or non-monotonic is of little relevance as what matters is the timing of the response. This coding strategy limits the potential that is available through the variety of amplitude responses produced at different odour concentrations that we and others have found. Both timing and amplitude provide useful information that can be employed in the neural coding of odour over different concentrations.

The present study used monomolecular odours, yet natural odours are often mixtures of different components that can interact antagonistically at the ORN receptor level (Inagaki et al., 2020; Xu et al., 2020; Zak et al., 2020). An odour mixture that causes antagonism in a particular OR type will make it less sensitive, while at the same time the mixture will increase the magnitude of lateral inhibition by activating other OR types. One prediction from our model is therefore that antagonized ORNs will result in MTC outputs that shift towards the D and DI categories, which necessarily changes the way MTCs code for that odour.

Conclusions

Our comparisons of input and output and mathematical modelling provide direct evidence of a functional transformation occurring in the OB. Non-monotonic concentration-response relationships in MTCs are common and expected given the ways that local and lateral inhibition can shape MTC activity. This transformation is likely to play a key role in facilitating odour discrimination and the ability for an animal to achieve perceptual concentration invariance.

Appendix

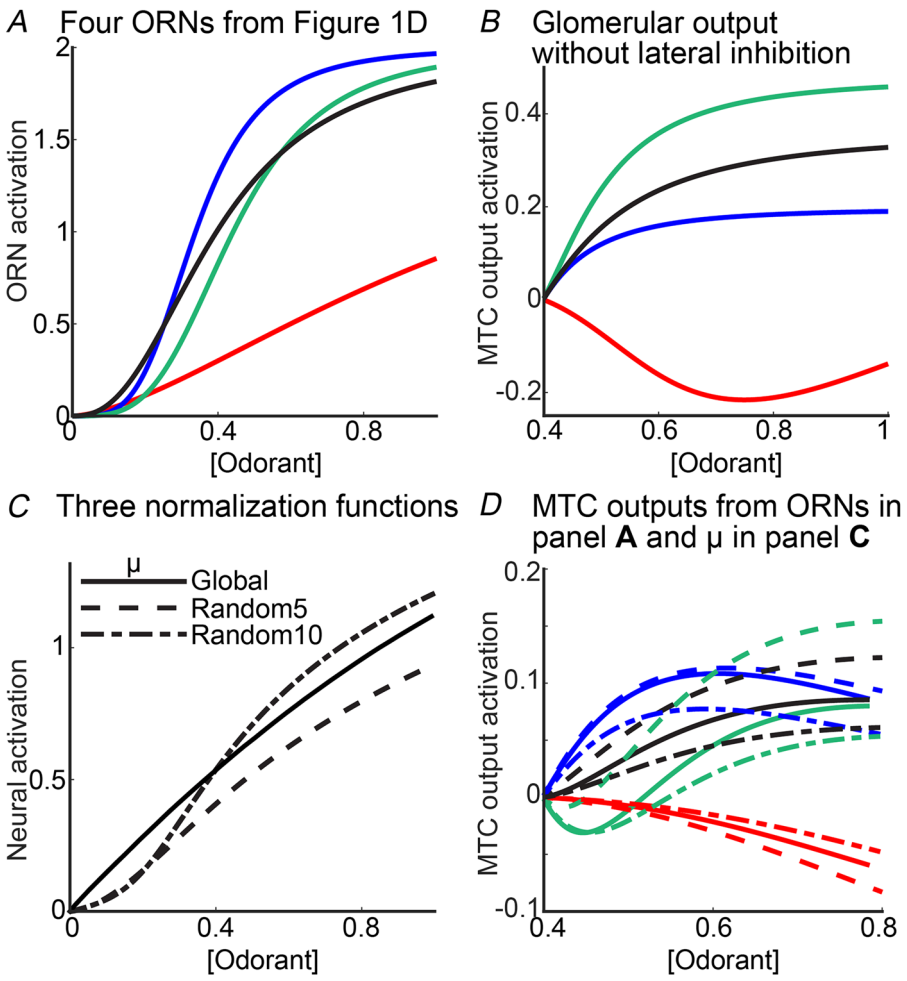

Figure A1. Input and output curves from the mathematical model
A, the four exemplar olfactory receptor neuron (ORN) concentration-response functions from Fig. 1*D*. *B*, the four inputs from panel *A* have been processed by the local inhibition circuit (only), resulting in three I and one DI mitral and tufted cell (MTC) response functions. Importantly no ID responses were generated in the absence of lateral inhibition. *C*, three different ORN functions used to implemental interglomerular processing. The solid 'μ_{global}' distribution is identical to the black dashed line in Fig. 1*C*. Randomly sampling and then averaging 5 and 10 signals from that figure's ORN population yielded the '$\mu_{Random5}$' and '$\mu_{Random10}$' distributions, respectively (different dashed lines). *D*, the four inputs from panel *A* processed using local inhibition and lateral inhibition implemented via the different functions in panel *C*. All four MTC categories were present irrespective of which population of ORNs was selected for interglomerular processing.

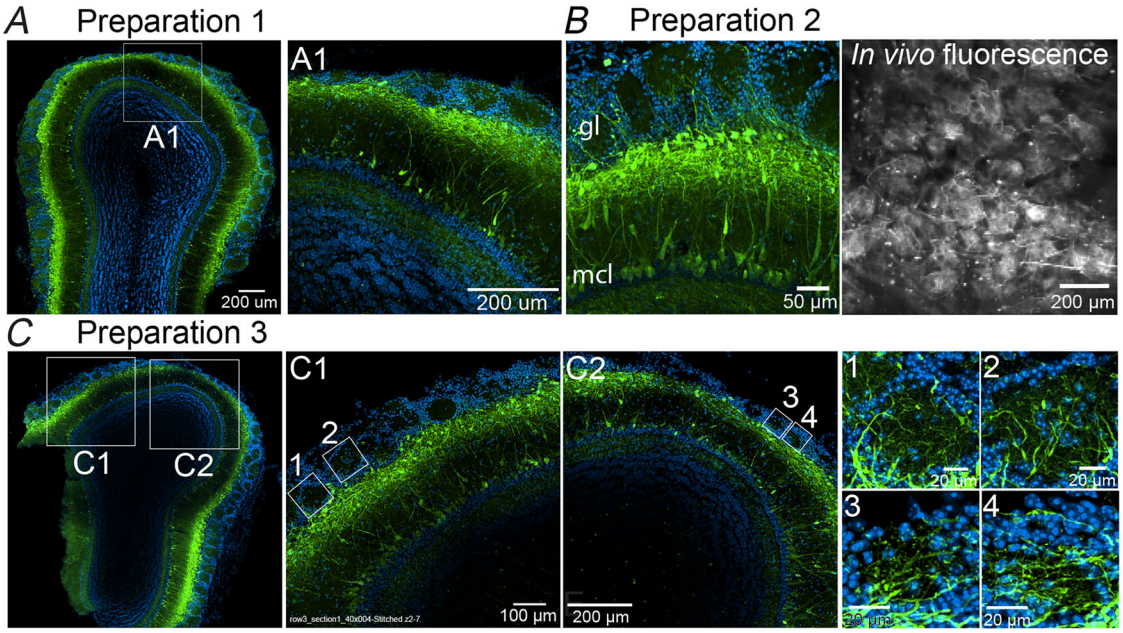

Figure A2. jGCaMP8m expression in the olfactory bulb (OB) in a cross between the Tbx21-cre and the TIGRE2-jGCaMP8m transgenic lines
A–C, images from three different mouse preparations. Panel *B* includes *in vivo* two-photon fluorescence from the glomerular layer from that preparation. Panel *C* includes cropped images of the glomerular layer with an adjusted colour lookup table. gl, glomerular layer; mcl, mitral cell layer.

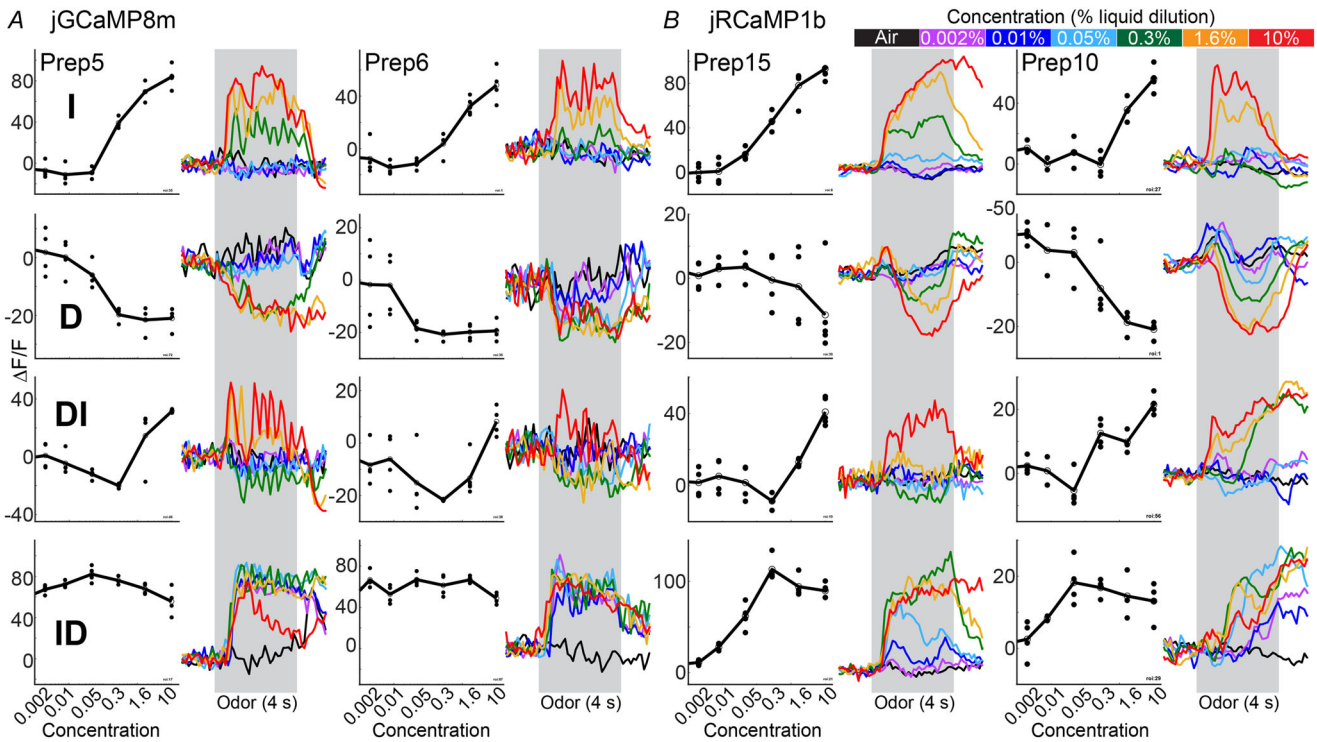

Figure A3. Imaging MTC glomeruli using jGCaMP8m
Mitral and tufted cell (MTC) glomerular responses with increasing, decreasing, decreasing–increasing and increasing–decreasing response categories, measured with jGCaMP8m (*A*) and jRCaMP1b (*B*).

References

Ackels, T., Erskine, A., Dasgupta, D., Marin, A. C., Warner, T. P. A., Tootoonian, S., Fukunaga, I., Harris, J. J., & Schaefer, A. T. (2021). Fast odour dynamics are encoded in the olfactory system and guide behaviour. *Nature*, **593**(7860), 558–563.

Akerboom, J., Chen, T.-W., Wardill, T. J., Tian, L., Marvin, J. S., Mutlu, S.ç, Calderón, N. C., Esposti, F., Borghuis, B. G., Sun, X. R., Gordus, A., Orger, M. B., Portugues, R., Engert, F., Macklin, J. J., Filosa, A., Aggarwal, A., Kerr, R. A., Takagi, R., … Looger, L. L. (2012). Optimization of a GCaMP calcium indicator for neural activity imaging. *Journal of Neuroscience*, **32**(40), 13819–13840.

Araneda, R. C., Kini, A. D., & Firestein, S. (2000). The molecular receptive range of an odorant receptor. *Nature Neuroscience*, **3**(12), 1248–1255.

Aungst, J. L., Heyward, P. M., Puche, A. C., Karnup, S. V., Hayar, A., Szabo, G., & Shipley, M. T. (2003). Centre-surround inhibition among olfactory bulb glomeruli. *Nature*, **426**(6967), 623–629.

Badura, A., Sun, X. R., Giovannucci, A., Lynch, L. A., & Wang, S. S. (2014). Fast calcium sensor proteins for monitoring neural activity. *Neurophotonics*, **1**(2), 025008.

Banerjee, A., Marbach, F., Anselmi, F., Koh, M. S., Davis, M. B., Garcia da Silva, P., Delevich, K., Oyibo, H. K., Gupta, P., Li, B. O., & Albeanu, D. F. (2015). An interglomerular circuit gates glomerular output and implements gain control in the mouse olfactory bulb. *Neuron*, **87**(1), 193–207.

Bischofberger, J., & Jonas, P. (1997). Action potential propagation into the presynaptic dendrites of rat mitral cells. *The Journal of Physiology*, **504**(Pt 2), 359–365.

Bozza, T., Feinstein, P., Zheng, C., & Mombaerts, P. (2002). Odorant receptor expression defines functional units in the mouse olfactory system. *Journal of Neuroscience*, **22**(8), 3033–3043.

Bozza, T., McGann, J. P., Mombaerts, P., & Wachowiak, M. (2004). In vivo imaging of neuronal activity by targeted expression of a genetically encoded probe in the mouse. *Neuron*, **42**(1), 9–21.

Braubach, O., Tombaz, T., Geiller, T., Homma, R., Bozza, T., Cohen, L. B., & Choi, Y. (2018). Sparsened neuronal activity in an optogenetically activated olfactory glomerulus. *Scientific Reports*, **8**(1), 14955.

Buck, L., & Axel, R. (1991). A novel multigene family may encode odorant receptors: A molecular basis for odor recognition. *Cell*, **65**(1), 175–187.

Burton, S. D., Brown, A., Eiting, T. P., Youngstrom, I. A., Rust, T. C., Schmuker, M., & Wachowiak, M. (2022). Mapping odorant sensitivities reveals a sparse but structured representation of olfactory chemical space by sensory input to the mouse olfactory bulb. *eLife*, **11**, e80470.

Carandini, M., & Heeger, D. J. (2011). Normalization as a canonical neural computation. *Nature Reviews Neuroscience*, **13**(1), 51–62.

Chae, H., Banerjee, A., Dussauze, M., & Albeanu, D. F. (2022). Long-range functional loops in the mouse olfactory system and their roles in computing odor identity. *Neuron*, **110**(23), 3970–3985.e3977.

Charpak, S., Mertz, J., Beaurepaire, E., Moreaux, L., & Delaney, K. (2001). Odor-evoked calcium signals in dendrites of rat mitral cells. *Proceedings of the National Academy of Sciences*, **98**(3), 1230–1234.

Chen, T. W., Wardill, T. J., Sun, Y., Pulver, S. R., Renninger, S. L., Baohan, A., Schreiter, E. R., Kerr, R. A., Orger, M. B., Jayaraman, V., Looger, L. L., Svoboda, K., & Kim, D. S. (2013). Ultrasensitive fluorescent proteins for imaging neuronal activity. *Nature*, **499**(7458), 295–300.

Chen, W. R., Midtgaard, J., & Shepherd, G. M. (1997). Forward and backward propagation of dendritic impulses and their synaptic control in mitral cells. *Science*, **278**(5337), 463–467.

Chen, W. R., Shen, G. Y., Shepherd, G. M., Hines, M. L., & Midtgaard, J. (2002). Multiple modes of action potential initiation and propagation in mitral cell primary dendrite. *Journal of Neurophysiology*, **88**(5), 2755–2764.

Chen, Y., Chen, X., Baserdem, B., Zhan, H., Li, Y., Davis, M. B., Kebschull, J. M., Zador, A. M., Koulakov, A. A., & Albeanu, D. F. (2022). High-throughput sequencing of single neuron projections reveals spatial organization in the olfactory cortex. *Cell*, **185**(22), 4117–4134.e4128.

Chong, E., Moroni, M., Wilson, C., Shoham, S., Panzeri, S., & Rinberg, D. (2020). Manipulating synthetic optogenetic odors reveals the coding logic of olfactory perception. *Science*, **368**(6497), eaba2357.

Christie, J. M., & Westbrook, G. L. (2003). Regulation of back-propagating action potentials in mitral cell lateral dendrites by A-type potassium currents. *Journal of Neurophysiology*, **89**(5), 2466–2472.

Cleland, T. A. (2010). Early transformations in odor representation. *Trends in Neuroscience*, **33**(3), 130–139.

Cleland, T. A., Johnson, B. A., Leon, M., & Linster, C. (2007). Relational representation in the olfactory system. *Proceedings of the National Academy of Sciences*, **104**(6), 1953–1958.

Cleland, T. A., & Sethupathy, P. (2006). Non-topographical contrast enhancement in the olfactory bulb. *BMC Neuroscience*, **7**, 7.

Daigle, T. L., Madisen, L., Hage, T. A., Valley, M. T., Knoblich, U., Larsen, R. S., Takeno, M. M., Huang, L., Gu, H., Larsen, R., Mills, M., Bosma-Moody, A., Siverts, L. A., Walker, M., Graybuck, L. T., Yao, Z., Fong, O., Nguyen, T. N., Garren, E., … Zeng, H. (2018). A suite of transgenic driver and reporter mouse lines with enhanced brain-cell-type targeting and functionality. *Cell*, **174**(2), 465–480 e422.

Dana, H., Mohar, B., Sun, Y., Narayan, S., Gordus, A., Hasseman, J. P., Tsegaye, G., Holt, G. T., Hu, A., Walpita, D., Patel, R., Macklin, J. J., Bargmann, C. I., Ahrens, M. B., Schreiter, E. R., Jayaraman, V., Looger, L. L., Svoboda, K., & Kim, D. S. (2016). Sensitive red protein calcium indicators for imaging neural activity. *eLife*, **5**, e12727.

Debarbieux, F., Audinat, E., & Charpak, S. (2003). Action potential propagation in dendrites of rat mitral cells in vivo. *Journal of Neuroscience*, **23**(13), 5553–5560.

Djurisic, M., Antic, S., Chen, W. R., & Zecevic, D. (2004). Voltage imaging from dendrites of mitral cells: EPSP attenuation and spike trigger zones. *Journal of Neuroscience*, **24**(30), 6703–6714.

Duchamp-Viret, P., Duchamp, A., & Chaput, M. A. (2000). Peripheral odor coding in the rat and frog: Quality and intensity specification. *Journal of Neuroscience*, **20**(6), 2383–2390.

Economo, M. N., Hansen, K. R., & Wachowiak, M. (2016). Control of mitral/tufted cell output by selective inhibition among olfactory bulb glomeruli. *Neuron*, **91**(2), 397–411.

Escabí, M. A., Higgins, N. C., Galaburda, A. M., Rosen, G. D., & Read, H. L. (2007). Early cortical damage in rat somatosensory cortex alters acoustic feature representation in primary auditory cortex. *Neuroscience*, **150**(4), 970–983.

Fantana, A. L., Soucy, E. R., & Meister, M. (2008). Rat olfactory bulb mitral cells receive sparse glomerular inputs. *Neuron*, **59**(5), 802–814.

Firestein, S., Picco, C., & Menini, A. (1993). The relation between stimulus and response in olfactory receptor cells of the tiger salamander. *The Journal of Physiology*, **468**(1), 1–10.

Firestein, S., & Zufall, F. (1993). Membrane currents and mechanisms of olfactory transduction. *Ciba Foundation Symposium*, **179**, 115–126.

Fukunaga, I., Berning, M., Kollo, M., Schmaltz, A., & Schaefer, A. T. (2012). Two distinct channels of olfactory bulb output. *Neuron*, **75**(2), 320–329.

Helassa, N., Podor, B., Fine, A., & Török, K. (2016). Design and mechanistic insight into ultrafast calcium indicators for monitoring intracellular calcium dynamics. *Scientific Reports*, **6**, 38276.

Higgins, N. C., Escabí, M. A., Rosen, G. D., Galaburda, A. M., & Read, H. L. (2008). Spectral processing deficits in belt auditory cortex following early postnatal lesions of somatosensory cortex. *Neuroscience*, **153**(2), 535–549.

Higgins, N. C., Storace, D. A., Escabí, M. A., & Read, H. L. (2010). Specialization of binaural responses in ventral auditory cortices. *Journal of Neuroscience*, **30**(43), 14522–14532.

Hu, X. S., Ikegami, K., Vihani, A., Zhu, K. W., Zapata, M., de March, C., Do, M., Vaidya, N., Kucera, G., Bock, C., Jiang, Y., Yohda, M., & Matsunami, H. (2020). Concentration-dependent recruitment of mammalian odorant receptors. *eNeuro*, **7**(2), ENEURO.0103-19.2019.

Huang, J. S., Kunkhyen, T., Rangel, A. N., Brechbill, T. R., Gregory, J. D., Winson-Bushby, E. D., Liu, B., Avon, J. T., Muggleton, R. J., & Cheetham, C. E. J. (2022). Immature olfactory sensory neurons provide behaviourally relevant sensory input to the olfactory bulb. *Nature Communications*, **13**(1), 6194.

Igarashi, K. M., Ieki, N., An, M., Yamaguchi, Y., Nagayama, S., Kobayakawa, K., Kobayakawa, R., Tanifuji, M., Sakano, H., Chen, W. R., & Mori, K. (2012). Parallel mitral and tufted cell pathways route distinct odor information to different targets in the olfactory cortex. *Journal of Neuroscience*, **32**(23), 7970–7985.

Inagaki, S., Iwata, R., Iwamoto, M., & Imai, T. (2020). Widespread inhibition, antagonism, and synergy in mouse olfactory sensory neurons In vivo. *Cell Reports* **31**(13), 107814.

Kapoor, V., Provost, A. C., Agarwal, P., & Murthy, V. N. (2016). Activation of raphe nuclei triggers rapid and distinct effects on parallel olfactory bulb output channels. *Nature Neuroscience*, **19**(2), 271–282.

Kato, H. K., Chu, M. W., Isaacson, J. S., & Komiyama, T. (2012). Dynamic sensory representations in the olfactory bulb: Modulation by wakefulness and experience. *Neuron*, **76**(5), 962–975.

Kikuta, S., Fletcher, M. L., Homma, R., Yamasoba, T., & Nagayama, S. (2013). Odorant response properties of individual neurons in an olfactory glomerular module. *Neuron*, **77**(6), 1122–1135.

Koldaeva, A., Zhang, C., Huang, Y. P., Reinert, J. K., Mizuno, S., Sugiyama, F., Takahashi, S., Soliman, T., Matsunami, H., & Fukunaga, I. (2021). Generation and characterization of a cell type-specific, inducible cre-driver line to study olfactory processing. *Journal of Neuroscience*, **41**(30), 6449–6467.

Lecoq, J., Tiret, P., & Charpak, S. (2009). Peripheral adaptation codes for high odor concentration in glomeruli. *Journal of Neuroscience*, **29**(10), 3067–3072.

Ma, M., Chen, W. R., & Shepherd, G. M. (1999). Electrophysiological characterization of rat and mouse olfactory receptor neurons from an intact epithelial preparation. *Journal of Neuroscience Methods*, **92**(1–2), 31–40.

Malnic, B., Hirono, J., Sato, T., & Buck, L. B. (1999). Combinatorial receptor codes for odors. *Cell*, **96**(5), 713–723.

McGann, J. P. (2013). Presynaptic inhibition of olfactory sensory neurons: New mechanisms and potential functions. *Chemical Senses*, **38**(6), 459–474.

Mitsui, S., Igarashi, K. M., Mori, K., & Yoshihara, Y. (2011). Genetic visualization of the secondary olfactory pathway in Tbx21 transgenic mice. *Neural Systems & Circuits*, **1**(1), 5.

Nagayama, S. (2010). Differential axonal projection of mitral and tufted cells in the mouse main olfactory system. *Frontiers in Neural Circuits*, **4**, 120.

Nagayama, S., Homma, R., & Imamura, F. (2014). Neuronal organization of olfactory bulb circuits. *Frontiers in Neural Circuits*, **8**, 98.

Nagayama, S., Takahashi, Y. K., Yoshihara, Y., & Mori, K. (2004). Mitral and tufted cells differ in the decoding manner of odor maps in the rat olfactory bulb. *Journal of Neurophysiology*, **91**(6), 2532–2540.

Niessing, J., & Friedrich, R. W. (2010). Olfactory pattern classification by discrete neuronal network states. *Nature*, **465**(7294), 47–52.

Olsen, S. R., Bhandawat, V., & Wilson, R. I. (2010). Divisive normalization in olfactory population codes. *Neuron*, **66**(2), 287–299.

Otazu, G. H., Chae, H., Davis, M. B., & Albeanu, D. F. (2015). Cortical feedback decorrelates olfactory bulb output in awake mice. *Neuron*, **86**(6), 1461–1477.

Parrish-Aungst, S., Shipley, M. T., Erdelyi, F., Szabo, G., & Puche, A. C. (2007). Quantitative analysis of neuronal diversity in the mouse olfactory bulb. *Journal of Comparative Neurology*, **501**(6), 825–836.

Petzold, G. C., Hagiwara, A., & Murthy, V. N. (2009). Serotonergic modulation of odor input to the mammalian olfactory bulb. *Nature Neuroscience*, **12**(6), 784–791.

Platisa, J., Zeng, H., Madisen, L., Cohen, L. B., Pieribone, V. A., & Storace, D. A. (2022). Voltage imaging in the olfactory bulb using transgenic mouse lines expressing the genetically encoded voltage indicator ArcLight. *Scientific Reports*, **12**(1), 1875.

Polley, D. B., Heiser, M. A., Blake, D. T., Schreiner, C. E., & Merzenich, M. M. (2004). Associative learning shapes the neural code for stimulus magnitude in primary auditory cortex. *Proceedings of the National Academy of Sciences*, **101**(46), 16351–16356.

Polley, D. B., Read, H. L., Storace, D. A., & Merzenich, M. M. (2007). Multiparametric auditory receptive field organization across five cortical fields in the albino rat. *Journal of Neurophysiology*, **97**(5), 3621–3638.

Polley, D. B., Steinberg, E. E., & Merzenich, M. M. (2006). Perceptual learning directs auditory cortical map reorganization through top-down influences. *Journal of Neuroscience*, **26**(18), 4970–4982.

Rabinowitz, N. C., Willmore, B. D., Schnupp, J. W., & King, A. J. (2011). Contrast gain control in auditory cortex. *Neuron*, **70**(6), 1178–1191.

Reisert, J., & Matthews, H. R. (1999). Adaptation of the odour-induced response in frog olfactory receptor cells. *The Journal of Physiology*, **519**(Pt 3), 801–813.

Rinberg, D., Koulakov, A., & Gelperin, A. (2006). Sparse odor coding in awake behaving mice. *Journal of Neuroscience*, **26**(34), 8857–8865.

Rothermel, M., Brunert, D., Zabawa, C., Díaz-Quesada, M., & Wachowiak, M. (2013). Transgene expression in target-defined neuron populations mediated by retrograde infection with adeno-associated viral vectors. *Journal of Neuroscience*, **33**(38), 15195–15206.

Rothermel, M., & Wachowiak, M. (2014). Functional imaging of cortical feedback projections to the olfactory bulb. *Frontiers in Neural Circuits*, **8**, 73.

Shen, Y., Banerjee, A., Albeanu, D. F., & Navlakha, S. (2025). An evolutionarily conserved scheme for reformatting odor concentration in early olfactory circuits. bioRxiv. https://doi.org/10.1101/2025.01.23.634259

Shusterman, R., Smear, M. C., Koulakov, A. A., & Rinberg, D. (2011). Precise olfactory responses tile the sniff cycle. *Nature Neuroscience*, **14**(8), 1039–1044.

Smear, M., Resulaj, A., Zhang, J., Bozza, T., & Rinberg, D. (2013). Multiple perceptible signals from a single olfactory glomerulus. *Nature Neuroscience*, **16**(11), 1687–1691.

Smear, M., Shusterman, R., O'Connor, R., Bozza, T., & Rinberg, D. (2011). Perception of sniff phase in mouse olfaction. *Nature*, **479**(7373), 397–400.

Storace, D. A., & Cohen, L. B. (2017). Measuring the olfactory bulb input-output transformation reveals a contribution to the perception of odorant concentration invariance. *Nature Communications*, **8**(1), 81.

Storace, D. A., & Cohen, L. B. (2021). The mammalian olfactory bulb contributes to the adaptation of odor responses: A second perceptual computation carried out by the bulb. *eNeuro*, **8**(5), ENEURO.0322-21.2021.

Storace, D. A., Cohen, L. B., & Choi, Y. (2019). Using genetically encoded voltage indicators (GEVIs) to study the input-output transformation of the mammalian olfactory bulb. *Frontiers in Cellular Neuroscience*, **13**, 342.

Subramanian, N., Leong, L. M., Salemi Mokri Boukani, P., & Storace, D. A. (2025). Recent odor experience selectively modulates olfactory sensitivity across the glomerular output in the mouse olfactory bulb. *Chemical Senses*, **50**, bjae045.

Sutter, M. L., & Loftus, W. C. (2003). Excitatory and inhibitory intensity tuning in auditory cortex: Evidence for multiple inhibitory mechanisms. *Journal of Neurophysiology*, **90**(4), 2629–2647.

Tian, L., Hires, S. A., Mao, T., Huber, D., Chiappe, M. E., Chalasani, S. H., Petreanu, L., Akerboom, J., McKinney, S. A., Schreiter, E. R., Bargmann, C. I., Jayaraman, V., Svoboda, K., & Looger, L. L. (2009). Imaging neural activity in worms, flies and mice with improved GCaMP calcium indicators. *Nature Methods*, **6**(12), 875–881.

Verhagen, J. V., Wesson, D. W., Netoff, T. I., White, J. A., & Wachowiak, M. (2007). Sniffing controls an adaptive filter of sensory input to the olfactory bulb. *Nature Neuroscience*, **10**(5), 631–639.

Vučinić, D., Cohen, L. B., & Kosmidis, E. K. (2006). Interglomerular center-surround inhibition shapes odorant-evoked input to the mouse olfactory bulb in vivo. *Journal of Neurophysiology*, **95**(3), 1881–1887.

Wachowiak, M., & Cohen, L. B. (2001). Representation of odorants by receptor neuron input to the mouse olfactory bulb. *Neuron*, **32**(4), 723–735.

Wachowiak, M., Dewan, A., Bozza, T., O'Connell, T. F., & Hong, E. J. (2025). Recalibrating olfactory neuroscience to the range of naturally occurring odor concentrations. *Journal of Neuroscience*, **45**(10), e1872242024.

Wachowiak, M., Economo, M. N., Díaz-Quesada, M., Brunert, D., Wesson, D. W., White, J. A., & Rothermel, M. (2013). Optical dissection of odor information processing in vivo using GCaMPs expressed in specified cell types of the olfactory bulb. *Journal of Neuroscience*, **33**(12), 5285–5300.

Watkins, P. V., & Barbour, D. L. (2008). Specialized neuronal adaptation for preserving input sensitivity. *Nature Neuroscience*, **11**(11), 1259–1261.

Wehr, M., & Zador, A. M. (2003). Balanced inhibition underlies tuning and sharpens spike timing in auditory cortex. *Nature*, **426**(6965), 442–446.

Wilson, C. D., Serrano, G. O., Koulakov, A. A., & Rinberg, D. (2017). A primacy code for odor identity. *Nature Communications*, **8**(1), 1477.

Xu, L., Li, W., Voleti, V., Zou, D. J., Hillman, E. M. C., & Firestein, S. (2020). Widespread receptor-driven modulation in peripheral olfactory coding. *Science*, **368**(6487), eaaz5390.

Yamada, Y., Bhaukaurally, K., Madarász, T.á. J., Pouget, A., Rodriguez, I., & Carleton, A. (2017). Context- and output layer-dependent long-term ensemble plasticity in a sensory circuit. *Neuron*, **93**(5), 1198–1212 e1195.

Yu, C. H., Yu, Y., Adsit, L. M., Chang, J. T., Barchini, J., Moberly, A. H., Benisty, H., Kim, J., Young, B. K., Heng, K., Farinella, D. M., Leikvoll, A., Pavan, R., Vistein, R., Nanfito, B. R., Hildebrand, D. G. C., Otero-Coronel, S., Vaziri, A., Goldberg, J. L., … Smith, S. L. (2024). The Cousa objective: A long-working distance air objective for multiphoton imaging in vivo. *Nature Methods*, **21**(1), 132–141.

Zak, J. D., Reddy, G., Konanur, V., & Murthy, V. N. (2024). Distinct information conveyed to the olfactory bulb by feedforward input from the nose and feedback from the cortex. *Nature Communications*, **15**(1), 3268.

Zak, J. D., Reddy, G., Vergassola, M., & Murthy, V. N. (2020). Antagonistic odor interactions in olfactory sensory neurons are widespread in freely breathing mice. *Nature Communications*, **11**(1), 3350.

Zavitz, D., Youngstrom, I. A., Borisyuk, A., & Wachowiak, M. (2020). Effect of interglomerular inhibitory networks on olfactory bulb odor representations. *Journal of Neuroscience*, **40**(31), 5954–5969.

Zhang, Y., Rózsa, M., Liang, Y., Bushey, D., Wei, Z., Zheng, J., Reep, D., Broussard, G. J., Tsang, A., Tsegaye, G., Narayan, S., Obara, C. J., Lim, J. X., Patel, R., Zhang, R., Ahrens, M. B., Turner, G. C., Wang, S. S., Korff, W. L., … Looger, L. L. (2023). Fast and sensitive GCaMP calcium indicators for imaging neural populations. *Nature*, **615**(7954), 884–891.

Zhou, Z., Xiong, W., Zeng, S., Xia, A., Shepherd, G. M., Greer, C. A., & Chen, W. R. (2006). Dendritic excitability and calcium signalling in the mitral cell distal glomerular tuft. *European Journal of Neuroscience*, **24**(6), 1623–1632.

Zhu, P., Frank, T., & Friedrich, R. W. (2013). Equalization of odor representations by a network of electrically coupled inhibitory interneurons. *Nature Neuroscience*, **16**(11), 1678–1686.

Additional information

Data availability statement

All data are available to *The Journal of Physiology* and interested parties upon reasonable request.

Competing interests

The authors declare no competing financial interests.

Author contributions

D.A.S. and R.B. were involved in the conception or design of the work. All authors were involved in the acquisition, analysis or interpretation of data for the work. D.A.S. and D.W. made the first drafts of all figures, and all authors were involved in revising them. D.A.S. wrote the first draft of the manuscript, and all authors were involved in revising it critically for important intellectual content. All authors approved the final version of the manuscript, agreed to be accountable for all aspects of the work in ensuring that questions related to the accuracy or integrity of any part of the work are appropriately investigated and resolved; and all persons designated as authors qualify for authorship, and all those who qualify for authorship are listed.

Funding

This study was funded by NIDCD R01 DC020519 (D.A.S.) and NIDCD DC000044 (D.W.).

Acknowledgements

We dedicate this paper to our mentor Lawrence B. Cohen, who always knew what to do. Thanks to Evan Lloyd and the members of the Storace laboratory for their thoughtful discussion of the manuscript.

Keywords

calcium imaging, concentration coding, mathematical model, olfactory bulb, transgenic mouse, two-photon

Supporting information

Additional supporting information can be found online in the Supporting Information section at the end of the HTML view of the article. Supporting information files available:

Peer Review History